samples were derived from malignant lymphoma patients without bone marrow involvement as described earlier.[24,25] Our analysis of *WT1*, *GATA-1* and *GATA-2* was approved by IRB (approved number 99) of the Nagoya University School of Medicine. Some leukemia cell lines were provided by Dr Hirokazu Nagai (National Hospital Organization, Nagoya Medical Center, Nagoya, Japan). Solid tumor cell lines with high *WT1* mRNA levels[8] were the generous gifts of Dr Haruo Sugiyama (Osaka University Graduate School of Medicine, Osaka, Japan).

Quantitative reverse transcriptase-PCR

Quantitative reverse transcriptase-PCR was performed as described.[24,25] *WT1* mRNA was measured using the Light Cycler system (Roche Diagnostics, Mannheim, Germany). Each primer set and PCR conditions have been described before.[24,25] *GATA-1*, *GATA-2* and glyceraldehyde-3-phosphate dehydrogenase (*GAPDH*) mRNAs were measured with a Power SYBR Green master mix using the ABI PRISM 7000 sequence detection systems (Applied Biosystems Japan Ltd, Tokyo, Japan). After producing first-strand cDNA, quantitative PCR was carried out using the following primer sets: *GATA-1*, forward 5'-CCCAAGAAGCGCCT GATTGT-3'; reverse 5'-GTGTAGCTTGTAGTAGAGGCCGC-3'. *GATA-2*, forward 5'-CGTTCCTGTTCAGAAGGC-3'; reverse 5'-G TTCTGCCCATTCATCTTGT-3'. *GAPDH*, forward 5'-CAGGAGC GAGATCCCTCCAA-3'; reverse 5'-CCCCCTGCAAATGAGCCC-3'. PCR conditions were GATA-1, 95 °C for 10 s followed by 56 °C for 15 s; GATA-2, 95 °C for 10 s followed by 56 °C for 15 s; and GAPDH, 95 °C for 10 s followed by 63 °C for 15 s. Forty cycles were used for *WT1*, *GATA-1*, *GATA-2* and *GAPDH*. *GAPDH* was used as the internal control for both clinical samples and cell lines. Relative mRNA was calculated as the respective mRNA/*GAPDH* mRNA in the log scale.

Western blotting

Western blotting of WT1, GATA-1, GATA-2 and Sp1 was carried out using the anti-WT1 antibody (clone 6F-H2, Dakocytomation, CA, USA), anti-GATA-1 (sc-265), anti-GATA-2 (sc-9008) and anti-Sp1 (sc-59) antibody (Santa Cruz Biotechnology Inc., Santa Cruz, CA, USA), respectively. We used the ECL chemiluminescence kit (Amersham Pharmacia Biotech, Buckinghamshire, UK) for signal detection.

Rapid amplification of 5' cDNA ends (5' RACE)

The transcription initiation point of *WT1* was determined as described in the Supplementary information.

Cloning of WT1 promoter and enhancer regions

We obtained an ~1.8-kb fragment covering the 5' region of exon1 of *WT1* using the 5' rapid amplification of cloned ends. This fragment was inserted into the *Kpn*-I and *Bgl*-II sites of pGL3 basic vector (Promega, Madison, WI, USA), and used for the promoter analysis (−1807/Luc). Truncation and mutation of *WT1* promoter were prepared by the PCR-based method. Similarly, the intron 3 and 3' enhancers of the *WT1* were also obtained by the PCR-based method. Production of the truncation and mutation of 5' promoter and enhancer is described in the Supplementary information.

Promoter and enhancer analysis

K562 (1×10^6), Jurkat (1×10^5), TYK-nu-cPr (1×10^5) and HepG2 (1×10^5) cells were transfected with 1 μg of reporter plasmid containing various lengths of the 5' promoter and/or enhancer region of *WT1* gene and 1 μg of β-galactosidase expression vector (Promega). The lipofectin reagent (Invitrogen, Carlsbad, CA, USA) was used for K562. The calcium precipitation method was used for TYK-nu-cPr and HepG2. Trans IT-Jurkat (Mirus Bio Co., Madison, WI, USA) was used for Jurkat cells. After 48 h, cell lysates were prepared. Luciferase activity was normalized with the β-galactosidase activity.

DNA transfection

Transfection of the expression vector was carried out using Trans IT-Jurkat, for Jurkat, and the calcium precipitation method for TYK-nu-cPr cells. *GATA-1* and *GATA-2* expression vectors were obtained from Dr Ritsuko Shimizu (Tsukuba University, Tochigi, Japan) and Dr Haruhiko Asano (Chubu University, Kasugai, Aichi, Japan), respectively. *GATA-1* cDNA or *GATA-2* cDNA was transferred into pcDNA3.1 vector (Invitrogen).

RNA interference

K562 cells (5×10^5) were transfected with small interfering RNA (siRNA) (final 100 nM) using Oligofectamine reagent (Invitrogen). GATA-1 siRNA (ID no. 3197) and GATA-2 siRNA (ID no. 145419) were purchased from Ambion (Austin, TX, USA). Scrambled siRNA was purchased from Dharmacon (GE Healthcare Sciences, Tokyo, Japan).

Electrophoresis mobility shift assay

Nuclear extract was prepared from K562, Jurkat, Daudi, HL-60, TYK-nu-cPr, Sw480, Az521 and HepG2 cells. Electrophoretic mobility shift assay (EMSA) was performed as described earlier.[26] For the supershift experiment, anti-GATA-1 or anti-GATA-2 antibody (Santa Cruz Inc.) was added to the nuclear extract for 30 min at room temperature before mixing with biotin-labeled probes as described below. Forward, 5'-CATTTA **TATC**AGCCGTTTT**TATC**TTTTCCTG-3'; reverse, 5'-CAGGAAA A**GATA**AAAACGGCT**GATA**TAAATG-3' (Bold letters are the GATA binding motifs). In some experiments, mutated oligo was used. Proximal-mutated GATA: forward, 5'-CATTT**CCAAA** AGCCGTTCCAAATTTTCCTG-3'; reverse, 5'-CAGGAAAAGT TTGGAACGGCT**TTTGG**AAATG-3'. Distal mutated GATA: forward, 5'-CATTTATATCAGCCGTT**CCAAA**TTTTCCTG-3'; reverse, 5'-CAG GAAAAG**TTTGG**AACGGCTGATATAAATG-3' (Bold letters are the mutated GATA binding sites). Biotin label was attached to the 3' end of each forward probe (Sigma Genosys, Hokkaido, Japan).

Chromatin immunoprecipitation assay

Chromatin immunoprecipitation assay was carried out as described earlier.[26] K562, Jurkat and TYK-nu-cPr cells were used for the crosslinking with formaldehyde. For the immunoprecipitation, normal mouse IgG, anti-GATA-1-antibody (Santa Cruz, final concentration; 3 μg/μl) or anti-GATA-2-antibody (Santa Cruz) was added and incubated at 4 °C overnight. Immunocomplexes were extracted and crosslinking was reversed by heating the elutes at 65 °C overnight. The eluates were then digested with proteinase K at 50 °C for 5 h and extracted with phenol/chloroform/isoamyl alcohol. DNA was purified by ethanol precipitation. The WT1 enhancer region was amplified by PCR using primers 5'-GGGAATTCGACTCATTTATATCAG CCGTTTT-3' (forward) and 5'-GGGTCGACCCTGGCTCTTTCC GACTC-3' (reverse).

Results and discussion

Correlation between mRNA levels of WT1 *and* GATA-1/GATA-2 *in acute leukemia clinical samples and cell lines*

In Figure 1, we analyzed 20 established leukemia cell lines to determine the correlation between *WT1* and *GATA-1/GATA-2* (Figures 1a and c). Seventy-five percent of the cell lines showed high mRNA expression (more than 10^{-3} of *GAPDH* mRNA), whereas others (such as Daudi and U937) showed a very low or undetectable level of *WT1* mRNA. *GATA-1* mRNA was observed in 10 out of the 20 cell lines analyzed, with the expression levels being heterogeneous. *GATA-2* mRNA was also observed in 13 out of those 20 cell lines. The correlation index between *WT1* and *GATA-1* or *WT1* and *GATA-2* was significant, suggesting a positive relationship between *WT1* and *GATA-1/-2* mRNA (Figure 1 lower part). The correlation between *GATA-1* and *GATA-2* mRNA was also positive. When we examined solid tumor cell lines (SW480, Az521 and TYK-nu-cPr), which express high *WT1* mRNA[8] (Figure 1b), we found that those cell lines with high *WT1* mRNA showed high *GATA-2*, but not *GATA-1* mRNA. We also found a high

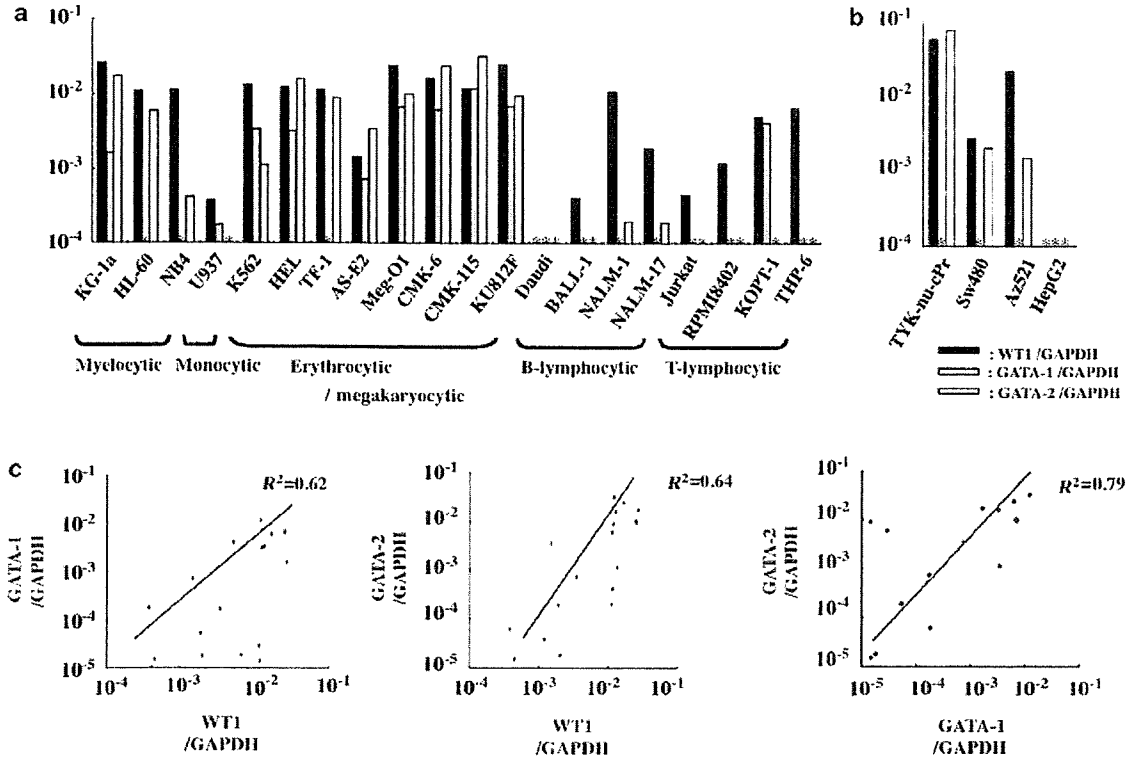

Figure 1 *WT1*, *GATA-1* and *GATA-2* mRNA in leukemia cell lines (**a**) and solid tumor cell lines (**b**). Relative *WT1*, *GATA-1* and *GATA-2* mRNA levels were examined by a quantitative reverse transcriptase-PCR. The internal control was *GAPDH*. The asterisks denote below the detection limit. The lower panels (**c**) show the correlation between *WT1* and *GATA-1*, *WT1* and *GATA-2*, and *GATA-1* and *GATA-2*, respectively.

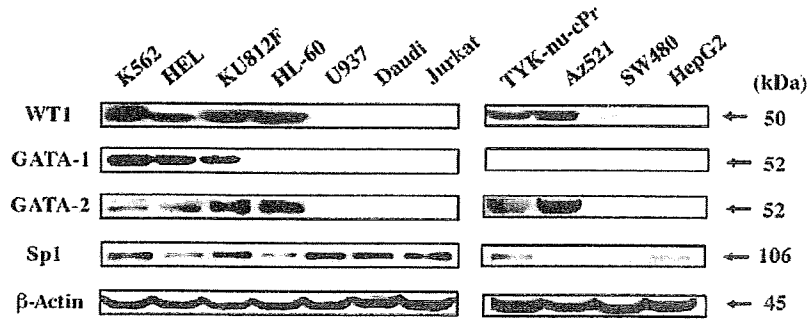

Figure 2 WT1, GATA-1, GATA-2 and Sp1 protein levels of representative cell lines. Left: Representative leukemia cell lines with high (K562, HEL, KU812F and HL60 cells) and low *WT1* mRNAs (U937, Daudi and Jurkat cells) were examined for their WT1, GATA-1, GATA-2 and Sp1 protein expressions by western blotting as described in Materials and methods. β-Actin was shown as the internal control. Right: solid tumor cell lines with high *WT1* mRNA (TYK-nu-cPr, Az521, SW480) as well as the negative control of HepG2 cells were analyzed for their WT1, GATA-1 and GATA-2 protein levels.

expression of *GATA-3* in Jurkat cells (data not shown), but its expression levels in the cell line panels were not examined further, as it was reported to express mainly in T lymphocytes and the embryonic brain.[27,28] We did not analyze *PAX* family genes because there are clear examples of tumor cell lines in which *PAX8* is not expressed but *WT1* is, or vice versa.[29,30]

Supplementary Figure 1 illustrates the relative mRNA levels of *WT1*, *GATA-1* and *GATA-2* from 23 AML and 3 ALL patient bone marrows. Most leukemia patients (85%) showed *WT1* mRNA levels of more than 10^{-2} of *GAPDH* mRNA, whereas the absence of *WT1* mRNA (below our detection limit) was observed only in one AML patient. *GATA-1* mRNA was very low in one AML case, whereas *GATA-2* mRNA was well observed in most. A low correlation index between *WT1* mRNA and *GATA-1/2* mRNA was obtained (data not shown) probably because of the heterogeneous percentage of blast cells within samples, and because of the remaining erythroid and megakaryocytic lineage cells.

We also examined *WT1*, *GATA-1* and *GATA-2* mRNA levels of both normal human hematopoietic stem cell fractions ($CD34^+$, $CD38^-$, Lin^-) and progenitor cell fractions ($CD34^+$, $CD38^+$, Lin^-) purified from two independent samples according to the method described in the Supplementary information. *WT1* mRNA levels of normal stem cell and progenitor cell fractions were significantly lower than those of AML samples with high *WT1* mRNA, whereas the *GATA-1* and *GATA-2* mRNA levels were almost equivalent to those of AML samples. In normal stem cell/progenitor cells, factors other than GATA-1/2 might also be relevant to their *WT1* mRNA expression. The contribution of GATA-1/2 to *WT1* mRNA expression of normal stem cell/progenitor cell fraction should be further analyzed in future experiments.

As to the *WT1* mRNA of the stem cell fraction, Hosen *et al.*[31] described the very low frequency of normal CD34-positive-hematopoietic progenitor cells with *WT1* mRNA level similar to those in leukemia cells. Our current study supports their results. Mouthon *et al.*[32] reported their *in situ* hybridization, suggesting the gradual increase of *GATA-1* mRNA from stem cells to immature erythroblasts and megakaryocytes. In our results, increase of *GATA-1* mRNA was observed from stem cell fraction to progenitor cell fraction. Furthermore, Maratheftis *et al.*[33] reported the upregulation of *GATA-1* mRNA of $CD34^+$ cells in myelodysplastic syndrome compared with that of normal control.

For precise and further analysis of a pure leukemia population, we used leukemia cell lines. Figure 2 illustrates the WT1, GATA-1, GATA-2 and Sp1 protein levels of representative cell lines with either high or low *WT1* mRNA. In these cell lines, WT1 protein levels were well correlated with *WT1* mRNAs. In WT1-high-leukemia cell lines, GATA-1 and GATA-2 protein levels were higher than those in WT1-low-leukemia cell lines. In the case of SW480, factors other than GATA1 and GATA2 might be involved in its WT1 expression.

5'-promoter analysis of WT1 *gene*

We determined the *WT1* transcription start site of K562 cells using the 5' rapid amplification of cloned ends method.[26] The

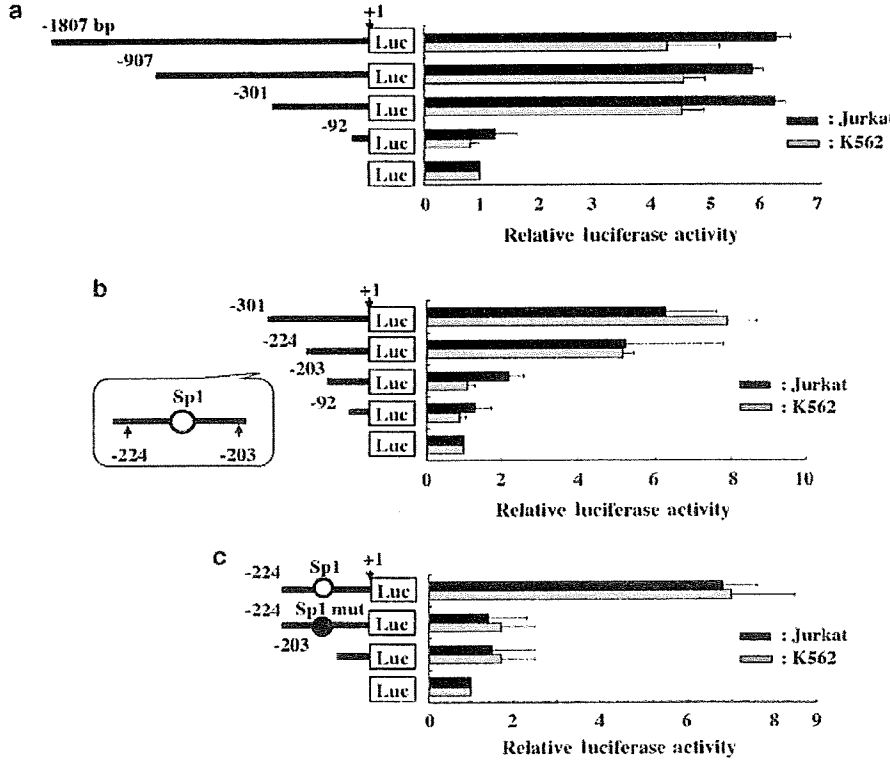

Figure 3 Promoter analysis of the 5' region of *WT1* gene. Using either K562 or Jurkat cells, the promoter activity of *WT1* gene was examined by transfecting the pGL3 basic reporter vector containing various lengths of the 5' promoter region as described in Materials and methods (**a**). Results were shown as the ratio of luciferase activity/β-gal. Data of pGL3 basic without 5' promoter were regarded as 1.0. The Sp1 site located between −224 and −203 bp is illustrated in (**b**). The solid circle in (**c**) shows mutated Sp1 site. The mean ± s.d. was calculated from three independent experiments.

start site of K562 cells was 185 bp downstream of the reported site in the National Center for Biotechnology Information database and 380 bp downstream of the one reported earlier.[13,14] On the basis of our result, we cloned the −1.8-kb region of *WT1* 5′ promoter. Figure 3 showed that the most potent promoter activity was located between −224 and −203 bp from exon 1 (Figures 3a and b). The introduction of a mutation into a putative Sp1 site in this region (Figure 3c) clearly showed this Sp1 site is essential for the 5′-promoter activity of *WT1*, which is consistent with the result of Cohen *et al.*[13] It also suggests that this promoter activity was not the sole determinant of the *WT1* expression, because K562 and Jurkat cells, which were associated with the high and low *WT1* expression, respectively (Figure 2), showed similar promoter activity, and the Sp1 protein level did not correlate with the WT1 protein level (Figure 2).

Enhancer analysis of WT1 *gene*

On the basis of results in Figures 2 and 3 as well as earlier reports suggesting the importance of intron 3 and 3′ enhancers,[15,20] we prepared luciferase reporter vectors containing −303 bp of the 5′-promoter region combined with the intron 3 and/or putative 3′ enhancer illustrated in Figure 4a. It is clear that the 3′ enhancer is potent in K562 cells with high *WT1* mRNA, but not in Jurkat or HepG2 cells with low *WT1* mRNA (Figure 4b). Interestingly, this 3′ enhancer was also active in TYK-nu-cPr cells, a solid tumor cell line with high *WT1* mRNA. In our analysis, the intron 3 enhancer did not play a major role in *WT1* gene expression, as was described earlier,[20] though some additive effect was detected in the presence of 3′ enhancer. We further analyzed 3′ enhancer by preparing various truncated forms of this region. Figure 4b showed that the distal region containing three out of six GATA sites was important. In earlier studies, Fraizer *et al.*[14] reported the importance of 3′ enhancer, and Wu *et al.*[15] confirmed their results using EMSA. However, the minimal responsive GATA site within this region has not been determined. Subsequent experiments using a mutated GATA motif introduced into these putative sites (Figure 4c) clearly showed that the minimal region in determining the total promoter/enhancer activity was the most distal GATA site of this enhancer.

The effects of transient expressions of *GATA-1* and *GATA-2* on *WT1* mRNA and *WT1* promoter and on WT1 protein of Jurkat and HepG2 cells are illustrated in Figure 5. *GATA-1* overexpression induced *WT1* mRNA in both Jurkat cells (1.9 times compared with mock-transfected cells) and HepG2 cells (2.0 times), whereas *GATA-2* overexpression increased WT1 mRNA in both Jurkat cells (1.7 times compared with mock-transfected cells) and HepG2 cells (2.4 times), respectively. *GATA*-induced WT1 protein expression was clearly observed in HepG2 cells (Figure 5b). The increase of WT1 protein in Jurkat

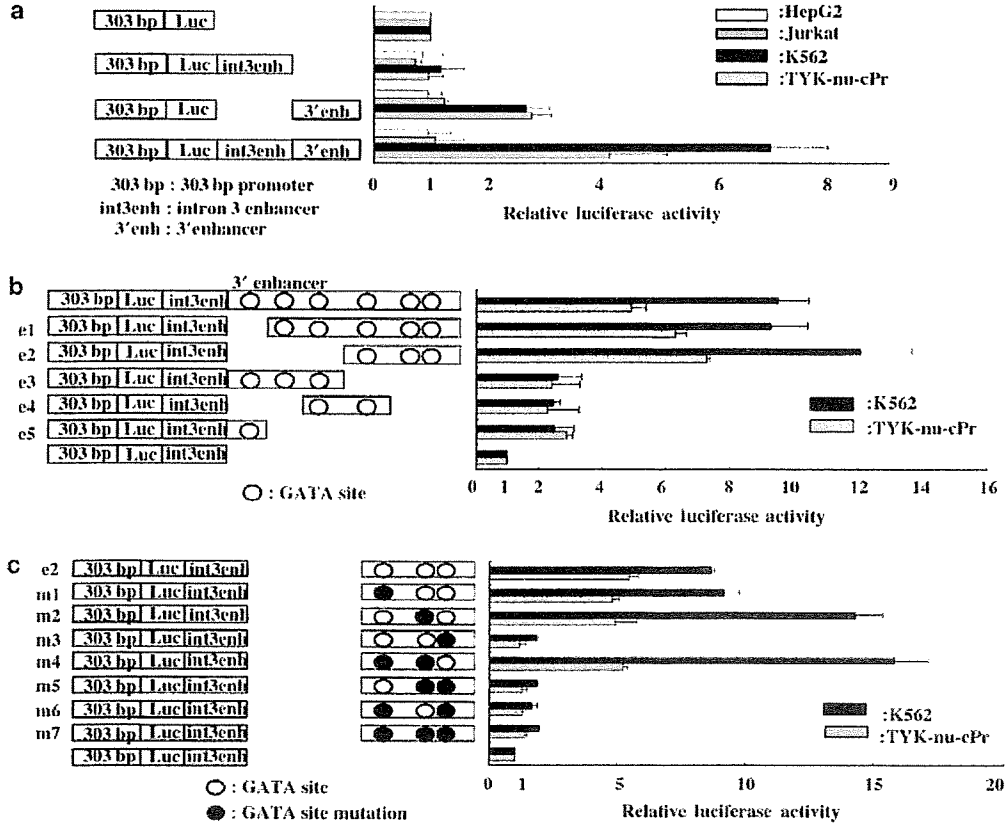

Figure 4 Effects of the intron 3 and 3′ enhancers of *WT1* gene. Effects of the intron 3 and 3′ enhancers were analyzed by luciferase reporter assay using various combinations of the promoter and enhancers as shown in (**a**) left. The sequence information was derived from earlier publications[14,15,20] and is described in Supplementary information. The mean ± s.d. was calculated from three independent experiments. Data of the relative luciferase activity of control vector (without enhancer elements) of each cell line were regarded as 1.0. In (**b** and **c**) deletion and mutation were introduced as illustrated in the left part of each panel. The open circle denotes wild-type GATA site, whereas the solid circle shows mutated GATA site. Data of the relative luciferase activity from luc vector containing only 5′ promoter and intron 3 enhancer were regarded as 1.0.

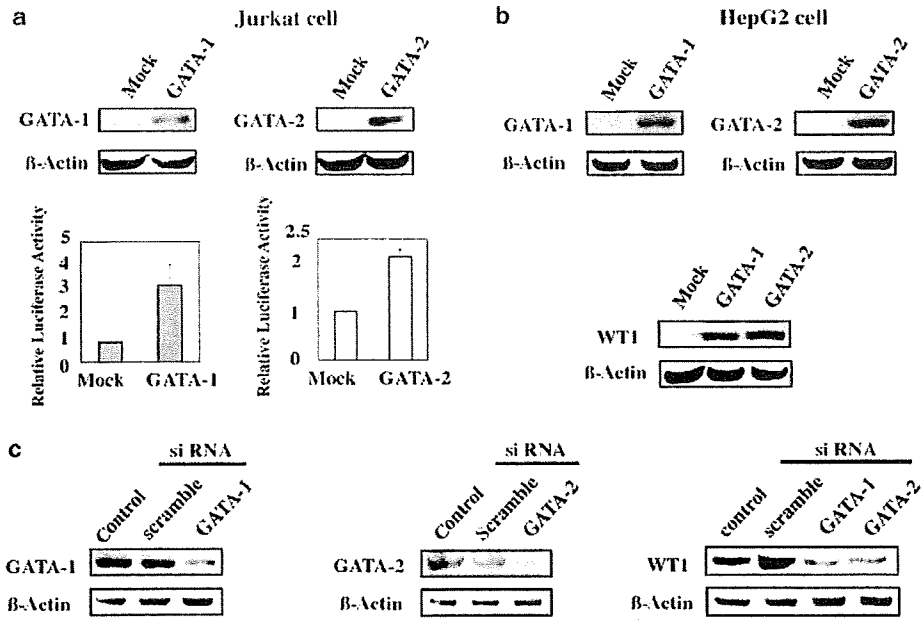

Figure 5 Effect of modulation of GATA family genes. *GATA-1* and *GATA-2* expression vectors were transiently introduced to Jurkat and HepG2 cells whose original *WT1* mRNA levels were low. Under overexpression conditions shown in the upper parts of **a** and **b**, we determined *WT1* promoter/enhancer activities using the e2 reporter of Figure 4c (**a**), or WT1 protein levels (**b**). Promoter/enhancer activity was expressed with the mock transfectant regarded as 1.0. (**c**) siRNAs of GATA-1 and GATA-2 were transfected as described in the Materials and methods. At 48 h after transfection, the WT1 protein level was evaluated by western blotting with β-actin as the internal control (right). Scramble siRNA was used as the control of the specificity of siRNAs used.

cells was only faintly detectable, probably because of the low transfection efficiency (data not shown). However, increased *WT1* promoter activity of Jurkat cells by transient *GATA-1* and *GATA-2* expression was clearly observed (Figure 5a). siRNA of *GATA-1* and *GATA-2* effectively inhibits WT1 expression (Figure 5c). Our quantitative reverse transcriptase-PCR, western blotting and promoter/enhancer analyses, and siRNA analysis showed that not only *GATA-1* but also *GATA-2* mRNA was expressed in both leukemia cell lines and clinical samples, and that GATA-1 and GATA-2 are equally effective in *WT1* gene expression by binding to a GATA site located in the 3'-enhancer region.

EMSA analysis of the distal GATA site of 3' enhancer

In EMSA, using the two most distal GATA sites (Figure 6a upper), several retarded bands (a, b, c and d) were observed in K562 nuclear extract, with smaller amounts in Jurkat and Daudi cells (Figure 6a lower). The intensities of the retarded bands were in proportion to their *WT1* mRNA levels (Figure 2). The cold competitor erased all the retarded bands supporting their specificity (Figure 6b left). The probe with a mutated distal GATA site (mut2), which is the same as m3 in Figure 4c, produced no retarded bands other than band d, suggesting that a, b and c bands are produced by GATA binding to the distal site (Figure 6c left); another probe with the mutated proximal GATA site (mut1) (described as m2 in Figure 4c) produced band patterns similar to those of wild-type probe (wt), supporting the results of our promoter analysis (Figure 4). Both anti-GATA-1 and anti-GATA-2 antibody to K562 nuclear extract inhibited bands a, b and c, suggesting that both GATA-1 and GATA-2 were the factors bound to this GATA site (Figure 6d upper).

We also examined solid tumors, TYK-nu-cPr and several other cell lines. EMSA of TYK-nu-cPr differed from those of k562 cells (Figure 6a lower-right). In addition to the commonly observed band d, we also observed bands e and f. They are also competed with the cold competitor (Figure 6b right). Interestingly, the band pattern of HL60 with GATA-2, but not GATA-1 expression, was similar to that of TYK-n-cPr (Figure 6a). The probe with the mutated GATA site (mut1), but not mut2, produced band e, which was reduced by anti-GATA-2 but not anti-GATA-1 antibody (Figures 6c and d).

The molecular weight and function of GATA-1 and GATA-2 were not markedly different. The difference observed in the EMSA pattern between K562 and TYK-nu-cPr was unexpected and quite interesting. Treatment with anti-GATA-1 and anti-GATA-2 antibodies showed that both GATA-1 and GATA-2 bound to the same GATA motif, and that GATA-2, but not GATA-1, was bound in TYK-nu-cPr cells. The complex formation between the GATA family and other cofactors might explain the different patterns observed. Further analysis is needed to elucidate the real binding mode of these GATA factors.

Chromatin immunoprecipitation assay using anti-GATA-1 and anti-GATA-2 antibodies

To confirm our EMSA data, a chromatin immunoprecipitation assay was carried out. Figure 7 shows that both GATA-1 and GATA-2 bound the 3' enhancer sequence in K562 cells, and that GATA-2, but not GATA-1, bound this enhancer in TYK-nu-cPr cells, a finding consistent with our promoter/enhancer analysis and EMSA data.

Conclusion

Taken together, these results showed that not only GATA-1[14,15] but also GATA-2 bound to the most distal GATA site of

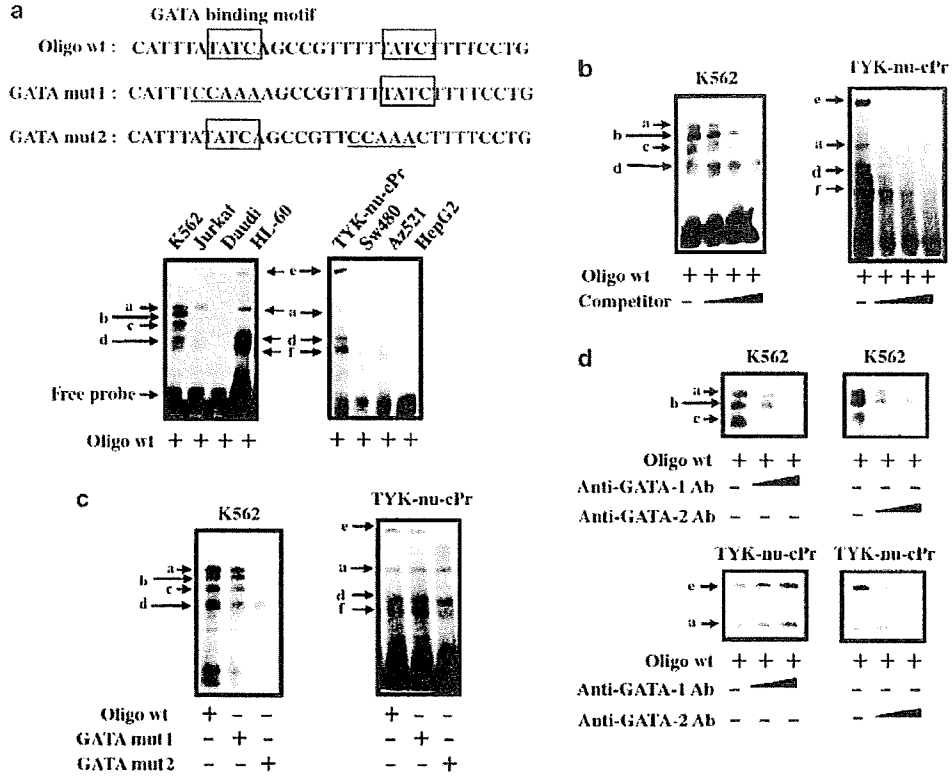

Figure 6 (**a**) EMSA analysis using probes covering the two distal GATA sites. Using biotin-labeled probes containing the two most distal GATA sites (oligo wild type, GATA mut1 and GATA mut2), the binding of transcription factor was examined using nuclear extracts from K562, Jurkat, Daudi, or HL60 cells (left) and TYk-nu-cPr, SW480, Az521 or HepG2 cells (right). Retarded bands were named a, b, c, d, e and f, respectively. (**b**) In addition to the labeled probe, a cold probe (x1–x10 excess) was added to the reaction mixture of K562 and TYK-nu-cPr cells, and EMSA was carried out. (**c**) A labeled probe with wild-type or with the mutated GATA site (GATA mut1 or GATA mut2 shown in (**a**) was used. (**d**) Anti-GATA-1 (final concentration: from 0.1 to 10 μg/ml) or anti-GATA-2 (final concentration: from 0.1 to 10 μg/ml) was added to nuclear extracts before incubation with the labeled DNA probe, as described in Materials and methods.

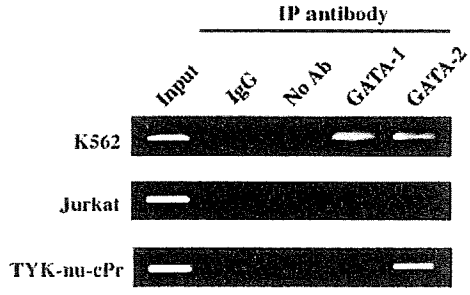

Figure 7 Chromatin immunoprecipitation assay was carried out as described in Materials and methods. After immunoprecipitation with anti-GATA-1 or anti-GATA-2 antibody, DNA was purified. PCR was performed using a primer set covering the region 123 bp long containing the two most distal GATA sites (Materials and methods). For specificity control, samples treated with unrelated IgG or PBS (no Ab) are also shown.

3′ enhancer, which was the important determinant of the *WT1* mRNA level in some cell lines. Furthermore, this 3′ enhancer is not unique to a hematopoietic lineage but has also proven effective in solid tumor cell lines. The regulatory mechanism of *WT1* gene expression described in these experiments provides the fundamental information on the WT1 biology of malignant diseases.

Acknowledgements

We express our sincere thanks to Dr H Nagai and Ms K Hagiwara (National Hospital Organization, Nagoya Medical Center, Nagoya, Japan) and to Dr Y Oji and Dr H Sugiyama (Osaka University Graduate School of Medicine, Osaka, Japan) for providing us with cell lines and useful comments. We acknowledge Ms Y Nomura for her excellent cell-sorting work. This work was supported in part by a Grant-in-Aid for Basic Research C 16590453 and by Health and Labour Research Grants from the Ministry of Health, Labour and Welfare, Japan.

References

1 Hewitt SM, Hamada S, McDonnell TJ, Rauscher III FJ, Saunder GF. Regulation of the proto-oncogenes bcl-2 and c-myc by the Wilms' tumor suppressor gene, *WT1*. *Cancer Res* 1995; **55**: 5386–5389.
2 Lou XN, Reddy JC, Yeyeti PL, Idris AH, Hosono S, Haber DA *et al*. The tumor suppressor gene *WT1* inhibits ras-mediated transformation. *Oncogene* 1995; **11**: 743–750.
3 Keilholz U, Menssen HD, Gaiger A, Menke A, Oji Y, Oka J *et al*. Wilms' tumour gene 1 (*WT1*) in human neoplasia. *Leukemia* 2005; **19**: 13181–13323.
4 Haber DA, Sohn RL, Buckler AJ, Pelletier J, Call KM, Housman DE. Alternative splicing and genomic structure of the Wilms tumor gene *WT1*. *Proc Natl Acad Sci USA* 1991; **88**: 9618–9622.

5 Loeb DM. WT1 influences apoptosis through transcriptional regulation of Bcl-2 family members. *Cell Cycle* 2006; **5**: 1249–1253.
6 Jomgeow T, Oji Y, Tsuji N, Ikeda Y, Ito K, Tsuda A *et al.* Wilms' tumor gene *WT1* 17AA(−)/KTS(−) isoform induces morphological changes and promotes cell migration and invasion *in vitro*. *Cancer Sci* 2006; **97**: 259–270.
7 Ito K, Oji Y, Tatsumi N, Shimizu S, Kanai Y, Nakazawa T *et al.* Antiapoptotic function of 17AA(+) *WT1* (Wilms' tumor gene) isoforms on the intrinsic apoptosis pathway. *Oncogene* 2006; **25**: 4217–4229.
8 Oji Y, Ogawa H, Tamaki H, Oka Y, Tsuboi A, Kim EM *et al.* Expression of the Wilms' tumor gene *WT1* in solid tumors and its involvement in tumor cell growth. *Int J Cancer Res* 1999; **90**: 194–204.
9 Boublikova L, Kalinova M, Ryan J, Quinn F, O'Marcaigh A, Smith O *et al.* Wilms' tumor gene 1 (*WT1*) expression in childhood acute lymphoblastic leukemia: a wide range of WT1 expression levels, its impact on prognosis and minimal residual disease monitoring. *Leukemia* 2006; **20**: 254–263.
10 Tamaki H, Ogawa H, Ohyashiki K, Ohyashiki JH, Iwama H, Inoue K *et al.* The Wilms' tumor gene *WT1* is a good marker for diagnosis of disease progression of myelodysplastic syndromes. *Leukemia* 1999; **13**: 393–399.
11 Weisser M, Kern W, Rauhut S, Schoch C, Hiddemann W, Haferlach T *et al.* Prognostic impact of RT-PCR-based quantification of *WT1* gene expression during MRD monitoring of acute myeloid leukemia. *Leukemia* 2005; **19**: 1416–1423.
12 Yang L, Han Y, Suarez Saiz F, Minden MD. A tumor suppressor and oncogene: the WT1 story. *Leukemia* 2007; **21**: 868–876.
13 Cohen HT, Bossone SA, Zhu G, McDonald GA, Sukhatme VP. Sp1 is a critical regulator of the Wilms' tumor-1 gene. *J Biol Chem* 1997; **272**: 2901–2913.
14 Fraizer GC, Wu YJ, Hewitt SM, Maity T, Yon CC, Huff V *et al.* Transcriptional regulation of the human Wilms' tumor gene (*WT1*): cell type-specific enhancer and promiscuous promoter. *J Biol Chem* 1994; **269**: 8892–8900.
15 Wu Y, Fraizer GC, Saunders GF. GATA-1 transactivates the WT1 hematopoietic specific enhancer. *J Biol Chem* 1995; **270**: 5944–5949.
16 Hosen N, Yanagihara M, Nakazawa T, Kanato K, Nishida S, Asada T *et al.* Identification of a gene element essential for leukemia-specific expression of transgenes. *Leukemia* 2004; **18**: 415–419.
17 Dehbi M, Pelletier J. PAX-8-mediated activation of the *wt1* tumor suppressor gene. *EMBO J* 1996; **15**: 4297–4306.
18 Siehl JM, Thiel E, Heufelder K, Snarski E, Schwartz S, Mailander V *et al.* Possible regulation of Wilms' tumour gene 1 (*WT1*) expression by the paired box genes PAX2 and PAX8 and by the haematopoietic transcription factor GATA-1 in human acute myeloid leukaemias. *Br J Haematol* 2003; **123**: 235–242.
19 Fraizer GC, Shimamura R, Zhang X, Saunders GF. PAX 8 regulates human WT1 transcription through a novel DNA binding site. *J Biol Chem* 1997; **272**: 30678–30687.
20 Zhang X, Xing G, Fraizer GC, Saunders F. Transactivation of an intronic hematopoietic-specific enhancer of the human Wilms' tumor 1 gene by GATA-1 and c-Myb. *J Biol Chem* 1997; **272**: 29272–29280.
21 Ohneda K, Yamamoto M. Roles of hematopoietic transcription factors GATA-1 and GATA-2 in the development of red blood cell lineage. *Acta Hematol* 2002; **108**: 237–245.
22 Weiss MJ, Orkin SH. GATA transcription factors: key regulators of hematopoiesis. *Exp Hematol* 1995; **23**: 99–107.
23 Shimamoto T, Ohyashiki K, Ohyashiki JH, Kawakubo K, Fujimura T, Iwama H *et al.* The expression pattern of erythrocyte/megakaryocyte-related transcription factor GATA-1 and the stem cell leukemia gene correlates with hematopoietic differentiation and is associated with outcome of acute myeloid leukemia. *Blood* 1995; **86**: 3173–3180.
24 Iwasaki T, Sugisaki C, Nagata K, Takagi A, Kojima T, Ito M *et al.* Wilms' tumor 1 message and protein expression in bone marrow failure syndrome and acute leukemia. *Pathol Int* 2007; **57**: 645–651.
25 Sobue S, Iwasaki T, Sugisaki S, Nagata K, Kikuchi R, Murakami M *et al.* Quantitative RT-PCR analysis of sphingolipid metabolic enzymes in acute leukemia and myelodysplastic syndromes. *Leukemia* 2006; **20**: 2042–2046.
26 Kikuchi R, Murakami M, Sobue S, Iwasaki T, Hagiwara K, Takagi A *et al.* Ewing's sarcoma fusion protein, EWS/Fli-1 and Fli-1 protein induce PLD2 but not PLD1 gene expression by binding to an ETS domain of 5′ promoter. *Oncogene* 2007; **26**: 1802–1810.
27 Ho IC, Vorhees P, Marin N, Oakley BK, Tsai SF, Orkin SH *et al.* Human GATA-3: a lineage-restricted transcription factor that regulates the expression of the T cell receptor alpha gene. *EMBO J* 1991; **10**: 1187–1192.
28 Ko L, Yamamoto M, Leonard MW, George KM, Ting P, Engel JD. Murine and human T-lymphocyte GATA-3 factors mediate transcription through a cis-regulatory element within the human T-cell receptor delta gene enhancer. *Mol Cell Biol* 1991; **11**: 2778–2784.
29 Tagge EP, Hanson P, Re GG, Othersen Jr HB, Smith CD, Garvin AJ. Paired box gene expression in Wilms' tumor. *J Pediatr Surg* 1994; **29**: 134–141.
30 Dressler GR, Douglas EC. Pax-2 is a DNA-binding protein expressed in embryonic kidney and Wilms tumor. *Proc Natl Acad Sci USA* 1992; **89**: 1179–1183.
31 Hosen N, Sonoda Y, Oji Y, Kimura T, Minamiguchi H, Tamaki H *et al.* Very low frequencies of human normal CD34+ haematopoietic progenitor cells express the Wilms' tumor gene WT1 at levels similar to those in leukemia cells. *Br J Haematol* 2002; **116**: 409–420.
32 Mouthon MA, Bernard O, Mitjavila MT, Romeo PH, Vainshenker W, Mathieu-Mahul D. Expression of tal-1 and GATA-binding proteins during human hematopoiesis. *Blood* 1993; **81**: 647–655.
33 Maratheftis CI, Bolaraki PE, Voulgarelis M. GATA-1 transcription factor is up-regulated in bone marrow hematopoietic progenitor CD34(+) and erythroid CD71(+) cells in myelodysplastic syndromes. *Am J Hematol* 2007; **82**: 887–892.

Supplementary information accompanies the paper on the Leukemia website (http://www.nature.com/leu)

The oral iron chelator deferasirox represses signaling through the mTOR in myeloid leukemia cells by enhancing expression of REDD1

Junko H. Ohyashiki,[1,3] Chiaki Kobayashi,[2] Ryoko Hamamura,[2] Seiichi Okabe,[2] Tetsuzo Tauchi[2] and Kazuma Ohyashiki[2]

[1]Intractable Diseases Therapeutic Research Center, Tokyo Medical University, Tokyo 160-0023; [2]First Department of Internal Medicine, Tokyo Medical University, Tokyo 160-0023, Japan

(Received December 11, 2008/Revised January 21, 2009/Accepted January 22, 2009/Online publication March 9, 2009)

To evaluate the effect of deferasirox in human myeloid leukemia cells, and to identify the moleclular pathways responsible for antiproliferative effects on leukemia cells during chelation therapy, we performed gene expression profiling to focus on the pathway involved in the anticancer effect of deferasirox. The inhibitory concentration (IC_{50}) of deferasirox was 17–50 μM in three human myeloid cell lines (K562, U937, and HL60), while those in fresh leukemia cells obtained from four patients it varied from 88 to 172 μM. Gene expression profiling using Affymerix GeneChips (U133 Plus 2.0) revealed up-regulation of cyclin-dependent kinase inhibitor 1A (*CDKN1A*) encoding $p21^{CIP}$, genes regulating interferon (i.e. *IFIT1*). Pathways related to iron metabolism and hypoxia such as growth differentiation factor 15 (*GDF-15*) and Regulated in development and DNA damage response (*REDD1*) were also prominent. Based on the results obtained from gene expression profiling, we particularly focused on the REDD1/mTOR (mammalian target of rapamycin) pathway in deferasirox-treated K562 cells, and found an enhanced expression of REDD1 and its down-stream protein, tuberin (TSC2). Notably, S6 ribosomal protein as well as phosphorylated S6, which is known to be a target of mTOR, was significantly repressed in deferasirox-treated K562 cells, and REDD1 small interfering RNA restored phosphorylation of S6. Although iron chelation may affect multiple signaling pathways related to cell survival, our data support the conclusion that REDD1 functions up-stream of tuberin to down-regulate the mTOR pathway in response to deferasirox. Deferasirox might not only have benefit for iron chelation but also may be an antiproliferative agent in some myeloid leukemias, especially patients who need both iron chelation and reduction of leukemia cells. (*Cancer Sci* 2009; 100: 970–977)

Iron plays a central role in the regulation of many cellular functions.[1] Evidence suggests that iron is required for cell survival and proliferation, and perturbation in cellular iron uptake can arrest cell growth both *in vitro* and *in vivo*.[2] As a part of ribonucleotide reductase, the enzyme responsible for deoxyribonucleotides synthesis, iron is an essential growth factor and rate-limiting trace element in DNA synthesis.[3] Dysregulaton of iron metabolism leads to iron overloading associated with deleterious effects on cells and tissues.[3] Numerous iron chelators have been synthesized in order to treat iron overload diseases, especially thalassemia. Evidence suggests the hyperproliferative effect of iron overload in a subset of cancer cells and iron depletion by chelators inhibits the proliferation of cancer cells, including leukemia cells.[4–8] Among the different molecules synthesized, hexadenate deferoxamine (DFO) is the major molecule used for the treatment of iron overload. However, it is highly hydrophilic, and inactive if taken perorally. For this reason, the perorally active iron chelator, deferasirox, is of special interest, since recent reports demonstrated that it acts as a potent nuclear factor kappa-light-chain-enhancer of activated B cell (NF-kappa-B) inhibitor and improves hematological data in a subset of patients with myelodysplastic syndromes (MDS).[9,10]

To evaluate the effect of deferasirox (also knows as ICL670, Novartis, Basel, Switzerland), and to identify molecular pathways responsible for the observed reduced transfusion requirement during chelation therapy, we performed gene expression profiling to focus on the pathway involved in the anticancer effect of deferasirox.

Materials and Methods

Reagents and cell cultures. The oral iron chelator, deferasirox was donated by Novartis. We purchased three human myeloid leukemia cell lines, K562, U937, and HL-60 from Health Science Research Resources Bank (Osaka, Japan) for this study. Cells were grown in RPMI1640 with 10% fetal bovine serum. After obtaining written informed consent, peripheral blood mononuclear cells (PBMCs) were isolated from four patients with acute myeloid leukemia (AML) by the Ficoll-Hypaque technique. This study was approved by our institutional medical ethics committee.

Cell viability and apoptosis assay. The inhibitory effect of deferasirox on cell growth was assessed by a Cell Counting Kit-8 (Wako Chemicals, Tokyo, Japan). Briefly, the cells (5000 cells/well) were incubated in triplicate in a 96-well plate in the presence or absence of indicated test samples at a final volume of 0.1 mL for 48 h at 37°C. Thereafter, 0.01 mL of tetrazolium salt, WST-1, was added to each well. After 2-h incubation at 37°C, the optical density (OD) at 450 nm was measured using a 96-well multiscanner autoreader with the extraction buffer used as a blank. Cell viability was expressed as a percentage (OD of the experiment sample/OD of the control × 100). Inhibitory concentration (IC_{50}) was calculated by GraphPad Prism 5 (GraphPad Software, La Jolla, CA, USA). For detection of apoptosis, caspase-3/7 activity was analyzed by the Caspase-Glo 3/7 assay (Promega, Madison, WI, USA). This test provides a pro-luminescent caspase-3/7 substrate, which contains the caspase-specific tetrapeptide sequence DEVD in a reagent, and determination of caspase and luciferase activity. The addition of a caspase-3/7 reagent results in cell lysis, followed by caspase-mediated cleavage of the Z-DEVD, release of luciferase reaction and finally the generation of luminescence.[11]

Gene expression and microarray data analysis. K562 cells were exposed to 10 μM or 50 μM (IC_{50} dose) of deferasirox for 24 h. After treatment, cells were harvested, and total RNA was extracted using an RNeasy Mini Kit (Qiagen, Germantown, MD, USA). The amount of RNA was measured by NanoDrop (NanoDrop Technologies, Wilmington, DE, USA), then the quality of extracted RNA was checked using a 2100 Bioanalyzer (Agilent Technologies, Wilmington, DE, USA). Gene expression profiling was done using the GeneChip U133 Plus 2.0 (Affymetrix, Santa Clara, CA, USA),

[3]To whom correspondence should be addressed. E-mail: junko@hh.iij4u.or.jp

doi: 10.1111/j.1349-7006.2009.01131.x

according to the manufacturer's instructions. Experiments were done in duplicate, and the microarray data were deposited in GEO (NCBI, Gene Expression Omnibus). For statistical analysis of gene expression, we utilized a GeneSifter® (geospiza, Seattle, WA, USA). Analysis of variance (ANOVA), and Student's *t*-test, were done using GeneSifter®. *P*-values of less than 0.05 were considered to indicate a statistically significant difference and the Benjamini-Hochberg algorithm was used for estimation of false discovery rates.[12]

Real-time reverse transcriptase polymerase chain reaction (RT-PCR). To confirm the microarray results, we performed RT-PCR by an ABI Prism 7700 Sequence Detection System (Applied Biosystems, Foster City, CA, USA) as we reported elsewhere.[13] We used Taqman gene expression assays for *REDD1* (Regulated in development and DNA damage response, assay ID: Hs00430304_gl; Applied Biosystems), and the amount of gene expression in each sample was evaluated as a percent of the standard curve generated from a serial dilution of quantitative PCR human reference total RNA (Stratagene, La Jolla, CA, USA). The obtained data from glyceraldehyde 3-phosphate dehydrogenase (*GAPDH*) were used to standardize the sample variation in the amount of input cDNA.

Immunoblotting. Cells were cultured for 24 h following respective treatments. Cells were washed twice in ice-cold phosphate-buffered saline (PBS) and cell pellets were lyzed in buffer containing 50 mM Tris-HCl (pH 7.5), 150 mM NaCl, 1% NP-40, 0.5% sodium dodecylsulfate (SDS) and a cocktail of protease inhibitors (Roche Diagnostics, Mannheim, Germany) at 4°C for 20 min. After centrifugation at 10000*g* for 20 min at 4°C, equal amounts of proteins were resolved by SDS-polyacrylamide gel electrophoresis (SDS-PAGE). The separated proteins were blotted onto a polyvinylidene difluoride (PDVF) membrane (Bio-Rad, Hercules, CA, USA). After blockage of non-specific binding sites with BlockAce (Dainippon-Sumitomo Pharma, Osaka, Japan), the filter was incubated with the following antibodies for 60 min at room temperature; REDD1 (Protein Tech Group, Inc., Chicago, IL, USA), tuberin (Santa Cruz Biotechnology, Santa Cruz, CA, USA), mammalian target of rapamycin (mTOR) (Cell Signaling, Denver, MA, USA), phosphorylated mTOR (S2448) (Cell Signaling), p70S6 kinase (Cell Signaling), phosphorylated S6 (Cell Signaling), and antiactin (Chemicon International Inc., Temecula, CA, USA). After washing, the blots were incubated for 60 min with horseradish peroxidase (HRP)-linked antimouse or antirabbit IgG (GE Healthcare, Buckinghamshire, UK). Signals were visualized using ECL Western blotting detection reagents and analysis system (GE Healthcare).

Small interfering RNA (siRNA). siRNA oligonucleotides for the REDD1 and GAPDH (control) were purchased from Thermo Scientific Dharmacon (Waltham, MA, USA) and resuspended in RNase-free-H_2O according to the manufacturer's instructions. K562 cells were transfected with REDD1 or control siRNA in the presence or absence of 50 μM of deferasirox. For cell transfection, approximately 1×10^6 cells were plated in 96-well plates to give 50% confluency. The cells were transfected with siRNA using a Gene Pulser electroporation system, then 48 h after transfection with REDD1 or control siRNA, deferasirox or dimethyl sulfoxide (DMSO) were added to the culture. The efficacy of transfection was evaluated by Western blotting as well as real-time RT-PCR as we reported elsewhere.[14]

Action of deferasirox in nude mice bearing transplantable human myelogenous leukemic cell line. For the *in vivo* assessment of deferasirox, 6-week-old female nude mice were injected with U937 cells and then assigned randomly to either the distilled water alone or deferasirox treatment groups. At 24 h after the injection, these mice were orally given either distilled water or deferasirox (50 mg/kg, daily) dissolved in distilled water. Mice were observed daily, and their body weight as well as signs of stress (e.g. lethargy, ruffled coat, or ataxia) were used to detect possible toxicities. The average tumor weight per mouse was calculated and used to analyze the group mean tumor weight ± SE ($n = 10$ mice). Tumors were collected at the predetermined times and fixed in paraformaldehyde.

Table 1. Inhibitory concentration of ICL670 (deferasirox) in human myeloid leukemia cells

Cells		Deferasirox (μM)
Cell lines	K562	46.33
	U937	16.91
	HL-60	50
Patient specimen	UPN1: post-MDS-AML	87.63
	UPN2: AML (M0)	92.17
	UPN3: AML(M4)	89.65
	UPN4: refractory AML (M5)	172.2

MDS, myelodysplastic syndromes; AML, acute myeloid leukemia.

Paraffin-embedded tissues were sectioned and processed for gross histopathology by hematoxylin–eosin staining or by the terminal deoxynuceotidyl transferase-mediated dUTP-biotin nick-end labeling (TUNEL) method to evaluate apoptosis.[15]

Results

Deferasirox-induced cell death in myeloid leukemia cells. We first examined the effects of deferasirox *in vitro* in various myeloid leukemia cells by a cell-counting assay. The median inhibitory concentration (IC_{50}) of deferasirox for K562 cells was 46.33 μM, that for U937 was 16.91 μM, that for HL-60 was 50 μM, respectively, and those for fresh leukemia cells obtained from four AML patients ranged from 87.63 to 172.2 μM (Table 1). To determine whether or not the cell death induced by deferasirox was due to apoptosis in myeloid leukemia cell lines, K562, U937, and HL60, we measured the activity of caspase-3/7 by a Caspase-Glo 3/7 kit (Promega). The number of viable cells were counted after 24 h exposure to deferasirox, in order to normalize the caspase-3/7 activity with respect to the number of cells per well. In all three leukemia cell lines tested, the activity of caspase-3/7 significantly increased after 50 μM deferasirox exposure (Fig. 1A–C). As shown in Fig. 1(D), the fold increase of apoptosis after normalization of cell numbers was evident in a dose-dependent manner.

Gene expression profile of deferasirox-treated K562 cells. To further understand how deferasirox induced cell death in human myeloid cells, K562 cells were treated with deferasirox or control for short time-periods, and microarray analysis was performed using a GeneChip (GEO, GPL570). Differential expression was analyzed using a GeneSifter®. All the microarray data was deposited in GEO (GSE11670: http://www.ncbi.nlm.nih.gov/geo/query/acc.cgi?token=fparzqkgqugqexi&acc=GSE11670). Up-regulated or down-regulated genes in deferasirox-treated K562 cells (expression level in the sample was 4-fold greater or lower than in untreated cells) are listed in Table 2. The salient features of up-regulated genes are summarized as follows. First, up-regulation of genes related to cell-cycle regulation was evident; cyclin G2 and cyclin-dependent kinase inhibitor 1A (*CDKN1A*) encoding p21, CDK-interacting protein1 (Cip). Second, genes regulating interferon were also up-regulated: interferon-induced protein with teteratricopeptide repeat 1 (*IFIT1*, *ISG56*), *IFIT3* (*ISG 60*), and interleukin 23 A (*IL23A*), which stimulate the production of interferon-γ. Third, genes related to apoptosis, such as *inhibin-β*, *B-cell lymphoma* (*BCL6*), pleckstrin homolog-like domain family A member 1 (*PHLDA1*), Bcl2/adenovirus E1B19-kDa protein-interacting protein 3-like (*BNIP3L*), tribbles homolog 3 (*TRIB2*), a negative regulator of NF-κB, were up-regulated. Fourth, growth differentiation factor 15 (*GDF15*), which is currently known as a negative regulator of the iron regulatory protein hepcidin, is remarkably up-regulated. Finally, it is notable that genes closely related to the oxygen regulatory system, including those regulated in development and DNA damage responses 1 (*REDD1*, also known as a HIF-1 responsive protein, RTP801), and phosphoglycerate

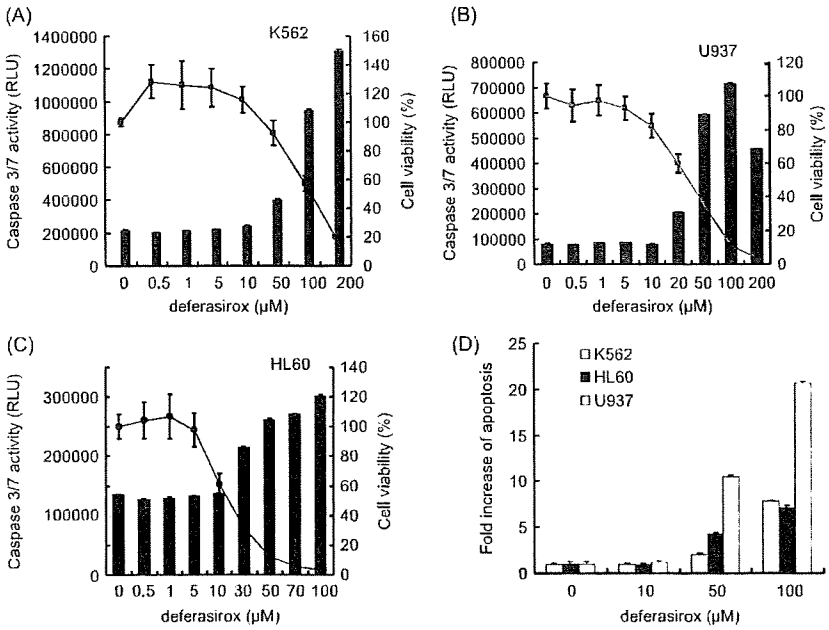

Fig. 1. Deferasirox-induced cell death in myeloid leukemia cell lines (A, K562; B, U937; C, HL60). Left *Y* axis indicates caspase 3/7 activity in IC_{50} dose of deferasiox-treated cell lines. The 'no cell' blank control value was subtracted from each reading. The percentage of viability is plotted with respect to untreated cells (right *Y* axis). The results are shown as means (±SD) percentage of viability from triplicate cultures with repeated experiments. (D) Caspase-3/7 activity is expressed relative to untreated control cells.

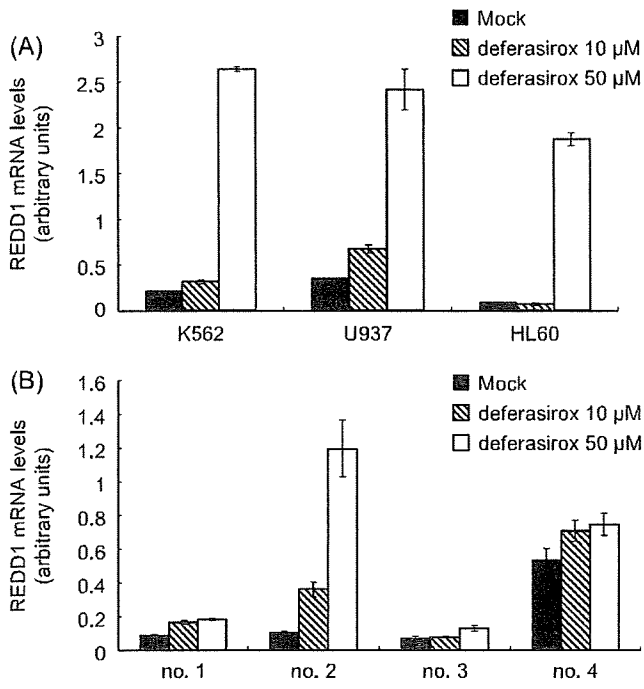

Fig. 2. Up-regulation of Regulated in development and DNA damage response (REDD1) expression in human myeloid leukemia cells. Relative REDD1 messenger RNA (mRNA) levels are determined using real time reverse transcription – polymerase chain reaction. The REDD1 gene expression level is normalized to the *GAPDH* mRNA levels as reported previously (Ref. no. 13). (A) The REDD1 gene expression is remarkably up-regulated in human myeloid leukemia cell lines. (B) REDD1 gene expression in fresh leukemia cells obtained from four patients.

dehydrogenase (*PHGDH*), which is related to NO metabolism, are up-regulated. Unlike up-regulated genes, we could not subdivide the extracted genes according to the molecular function; however, we found down-regulation of solute carrier family 5 member 6 (*SLC5A6*), which is related to iron-transport.

Up-regulation of *REDD1* in deferasirox-treated myeloid leukemia cells. Based on the results obtained from the differential expression pattern, we particularly focused our study on a gene closely related to oxygen regulation, *REDD1*. To determine whether up-regulation of *REDD1* takes place ubiquitously in the antitumor activity of deferasirox, we examined the change of *REDD1* expression by real-time RT-PCR in three human myeloid leukemia cell lines. Cells were treated with or without deferasirox (10 μM and 50 μM) for 24 h, and total RNA was collected. The *REDD1* expression remarkably increased after deferasirox treatment with a more than 2-fold increase of *REDD1* expression at 50 μM deferasirox, in all three leukemia cell lines (Fig. 2A). We also examined *REDD1* expression in four samples obtained from AML patients. Although the degree of increased *REDD1* expression varies among the samples, *REDD1* expression was up-regulated after deferasirox treatment in some freshly obtained samples from AML patients (Fig. 2B).

REDD1 suppresses S6 ribosomal protein via mTOR pathways. We therefore focused on the REDD1/TSC (tuberous sclerosis complex) pathway, which modulate mTOR signaling. An important mechanism through which mTOR signaling is regulated involves the Tuberin-Hamartin complex. We found up-regulation of TSC2 (tuberin) in accordance with REDD1 in deferasirox-treated K562 cells (Fig. 3A). Since TSC1 is regulated by V-AKT murine thymoma viral oncogene homolog 1 (AKT), we also examined the AKT expression in deferasirox-treated K562 cells. However, AKT protein expression was not altered after deferasirox treatment (data not shown). This indicates that TSC2 is up-regulated through the REDD1/TSC2 pathway, rather than the AKT/TSC2 pathway. Subsequently, phosphorylated mTOR, and phosphrylated-p70S6kinase, decreased in a dose-dependent manner (Fig. 3A,B). We noted a dose-dependent decrease of phophorylated-S6 protein, which is known as a downstream effecter of mTOR, in K562 cells treated with 50 μM of deferasirox (Fig. 3A bottom), indicating that deferasirox inhibits ribosomal S6 via mTOR pathway in K562 cells. Down-regulation of phosphorylated ribosomal S6 protein was also found in deferasirox-treated U937 and HL60 cells (Supporting File S1).

Inhibition of REDD1 resutores S6 ribosomal protein. To assess whether or not the enhanced expression of REDD1 mRNA was necessary for repression of mTOR signaling, siRNAs direct against the human REDD1 mRNA were used to reduce its expression in K562 cells in the presence or absence of deferasirox. Treatment

doi: 10.1111/j.1349-7006.2009.01131.x

Table 2. Genes altered in deferasirox-treated K562 cells

No.	Gene ID	Gene name	Molecular function	*P*-value
I. Up-regulated genes in deferasirox-treated K562 cells				
1	INHBE	Inhibin beta E	Hormone activity	0.00051
2	IFIT1	Interferon-induced protein with tetratricopeptide repeats 1, ISG56	Immune response	0.000906
3	MYEF2	Myeloin expression factor 2	Transcription	0.000224
4	REDD1	Regulated in development and DNA damage responsed 1,DNA damage-inducible transcript 4, DDIT4, HIF1-responsive protein RTP801	Inhibitor of mtor pathway	0.000027
5	PHGDH	Phosphoglycerate dehydrogenase	L-serine biosynthetic process; regulation of oxideructase activity (Redox)	0.000002
6	ATF3	Activating transcription factor 3	Regulation of transcription, DNA-dependent	0.000016
7	TP53INP1	P53-dependent damage-inducible nuclear protein 1	P53-dependent apoptosis	0.001184
8	ASNS	Asparagine synthetase	Asparagine biosynthetic process; NO metabolism	0.000063
9	GDF15	Growth differentiation factor 15	Signal transduction; TGF beta family	0.000003
10	IL8	Interleukin 8	Angiogenesis	0.000298
11	CTH	Cystathionase (cystathionine gamma-lyase)	Amino acid biosynthetic process	0.000034
12	MYO5A	Myosin VA (heavy polypeptide 12, myoxin)	Transport	0.000445
13	GADD153	DNA-damage-inducible transcript 3, DDIT3	Cell cycle arrest	0.000344
14	MAPKAPK5	Mitogen-activated protein kinase-activated protein kinase 5	Protein amino acid phosphorylation	0.000489
15	BCL6	B-cell CLL lymphoma 6	Protein import into nucleus, translocation	0.000156
16	PMAIP1	Phorbol-12-myristate-13-acetate-induced protein 1	Release of cytochrome c from mitochondria	0.000019
17	CCNG2	Cyclin G2	Regulation of progression through cell cycle	0.000653
18	HPSE	Heparanase precursor	Proteoglycan metabolic process	0.000714
19	CDKN1A	Cyclin-dependent kinase inhibitor 1 A (p21, Cip1)	Response to DNA damage stimulus	0.000104
21	PHLDA1	Pleckstrin homology-like domain, family A, member 1	Apoptosis	0.000129
22	BNIP3L	Bcl2/adenovirus E1B 19-kdprotein-interacting protein 3-like	Apoptosis	0.000146
23	NR4A1	Nuclear receptor subfamily 4, group A, member 1	Transcription: MAPK signaling	0.000739
24	IFIT3	Interferon-induced protein with tetratricopeptide repeats 3, ISG 60	Immune response	0.000355
25	IL23A	Interleukin 23-alpha	Inflammatory response; stimulate the production of interferon-gamma (ifng)	0.000503
26	IGF1	Insulin-like growth factor 1 (somatomedin C)	Skeletal development	0.000059
27	TRIB3	Tribbles homolog 3 (Drosophila)	Negative regulator of NF-kappaB	0.000409
II. Down-regulated genes in ICL670 treated K562 cells				
28	TNFSF13B	Tumor necrosis factor ligand superfamily, member 13	B cell homeostasis	0.001076
29	LYAR	cDNA DKFZp434G0514	Protein binding	0.000295
30	SLC5A6	Solute carrier family 5 (sodium-dependent vitamin transporter), member 6 (SLC5A6)	Ion transport	0.000018
31	PCDH12	Protocadherin 12	Cell adhesion	0.000589
32	EVI1	Ecotropic viral integration site 1	Multicellular organismal development	0.001132
33	FABP5	Fatty acid binding protein 5 (psoriasis-associated)	Lipid metabolic process	0.000627
34	RLBP1	Retinaldehyde-binding protein 1	Vitamin a metabolic process	0.000011
35	DRD1	D-1 dopamine receptor	Signal transduction	0.000388
36	CDH7	Cadherin 7	Homophilic cell adhesion	0.000282
37	CCDC14	cDNA clone ZE16C03	Electron transport	0.000862
38	CCDC39	cDNA DKFZp434A128	Mitochondrion	0.000062

of REDD1 siRNA caused a reduction in REDD1 expression to ~50% of the value observed in untreated cells or cells that had been treated with control siRNA (Fig. 4A). Moreover, treatment of REDD1 siRNA prior to deferasirox dramatically attenuated the drug-induced expression of REDD1 (Fig. 4B). Notably, deferasirox-induced decrease in S6K1 phosphorylation was blocked by REDD1 siRNA treatment. In contrast, the control siRNA had no effect on the deferasirox-induced decrease in S6K1 phosphorylation.

Deferasirox supresses heterotransplated tumor growth in nude mice bearing myeloid leukemia cells. To further study the activity of deferasirox on tumor growth *in vivo*, we tested a mouse model of human myeloid leukemia. Subcutaneous injection of U937 cells into nude mice resulted in an aggressive malignancy resembling acute leukemia, characterized by tumor, splenomegaly, and invasion of leukemia cells into hematopoietic and non-hematopoietic tissue: some of them had ascites without obvious tumor formation at the injected area. The control mice (distilled water alone) died of a condition resembling acute leukemia or tumor-bearing by 50 days; however, 2/10 mice treated with deferasirox survived for more than 90 days; deferasirox-treated mice tended to survive longer than those with saline ($P = 0.2450$) (Fig. 5A). The tumor volume of the subcutaneous tumors was significantly smaller in mice treated by deferasirox compared to those with vehicle alone ($P < 0.0001$) (Fig. 5B). No deferasirox-treated mice showed any adverse events. Histopathological analysis of xenotransplant mice revealed infiltration of the spleen and bone marrow with leukemic blasts. In contrast, deferasirox-treated mice demonstrated distinct morphological changes, including condensed nucleoli and an increasing number of apoptotic cells detected by the TUNEL method (Fig. 5C). These results indicate that deferasirox yields a desirable therapeutic index that can reduce the *in vivo* growth of myeloid leukemia cells in an efficacious manner.

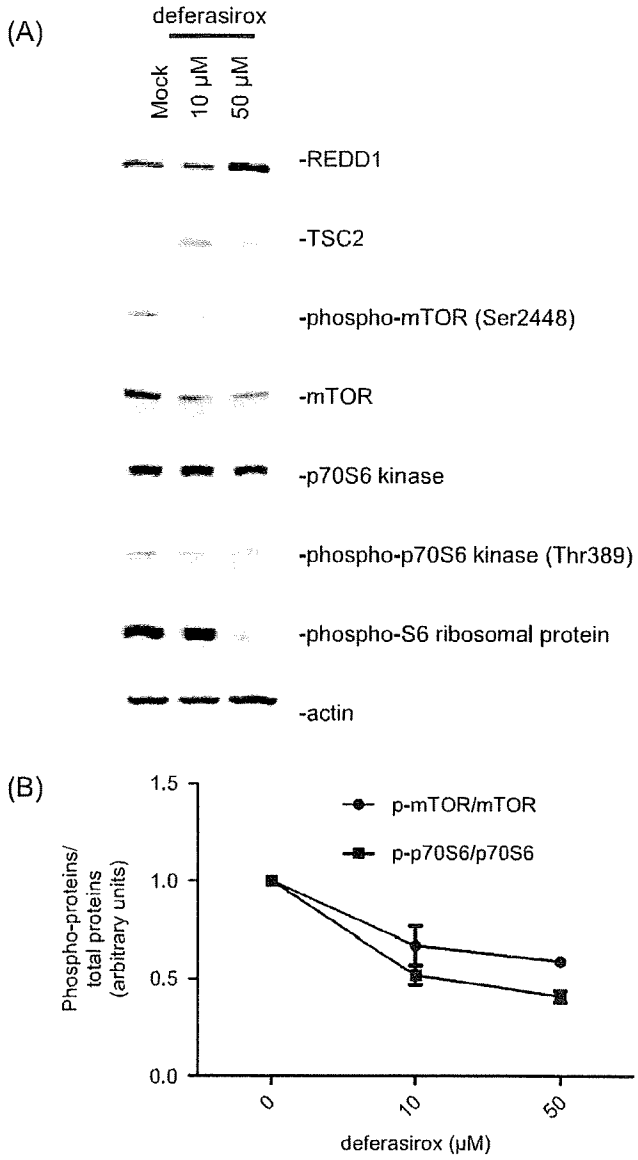

Fig. 3. Western blot analysis of K562 cells with or without treatment by deferasirox (10 μM and 50 μM). (A) Expression of Regulated in development and DNA damage response (REDD1) and tuberous sclerosis complex 2 (TSC2) are increased in deferasirox-treated K562 cells. Phosphorylated mammalian target of rapamycin (mTOR), phosphorylated-p70S6 kinase and phosphorylated S6 ribosomal protein, were decreased in a dose-dependent manner. (B) The intensity of signals were measured by a Versa-Doc gel imaging system (Bio-Rad Laboratories, Hercules, CA, USA). The ratio of phophorylated protein per total protein is expressed as an arbitrary unit. We confirmed the dose-dependent decrease of phosphorylated mTOR and phophorylated-p70S6 proteins in deferasirox-treated K562 cells.

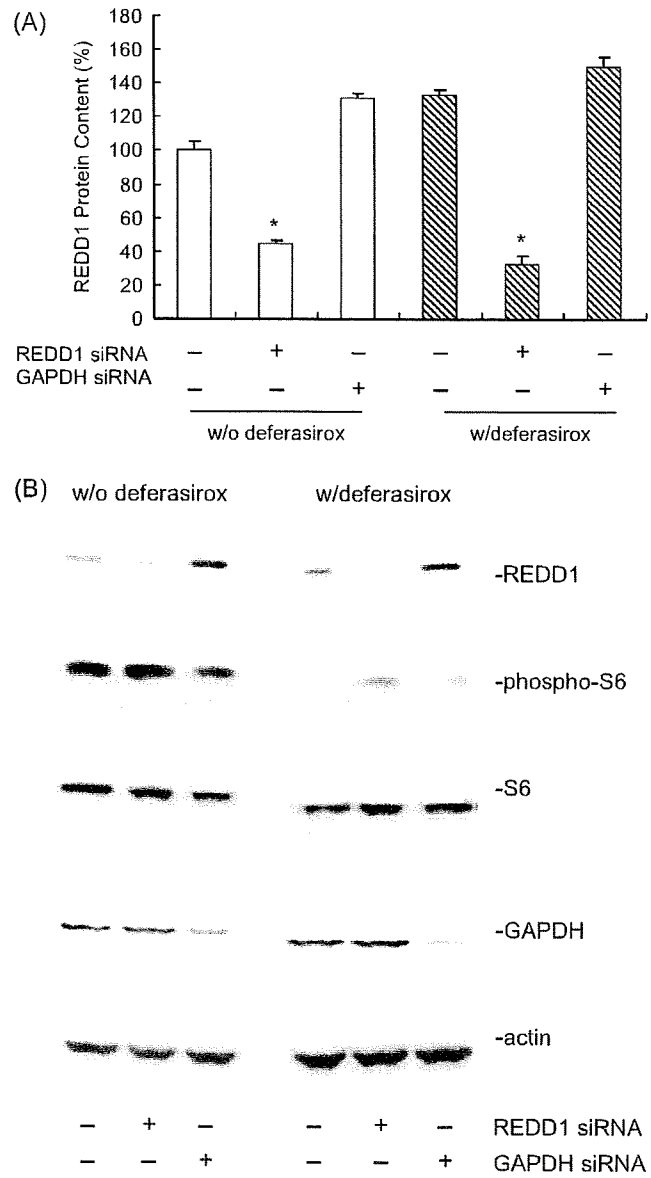

Fig. 4. Inhibition of Regulated in development and DNA damage response (REDD1) by small interfering RNA (siRNA) in the presence or absence of deferasirox in K562 cells. (A) REDD1 siRNA induced phosphorylation of S6 ribosomal protein in cells with or without deferasirox. However, the effect was more evident in deferasirox-treated K562 cells. (B) REDD1 protein contents are expressed as a percent with respect to untreated cells. Administration of REDD1 siRNA caused a reduction in REDD1 expression up to 50% of the value observed in untreated cells or cells that had been administrated a control glyceraldehyde 3-phosphate dehydrogenase (GAPDH) siRNA.

Discussion

We set out to determine the moleclular pathways responsible for antiproliferative effects on human myeloid leukemia cells during chelation therapy. The antiproliferative effect of iron chelating agents has been well recognized.[4,7,16–18] However, in the past, the exact mechanism of the antineoplastic effects of iron chelator were not clearly determined. Among iron chelators, deferasirox has been shown to have higher antiproliferative effects by apoptosis in cultured human hepatocytes and hepatocellular carcinoma cell lines than O-trensox,[19,20] and deferasirox is now available as an oral iron chelator. Chantrel-Graussard *et al.* further demonstrated that deferasirox induced cell cycle blockade in the G2-M phase and inhibited polyamine biosynthesis by decreasing ornithine decarboxylase and spermidine N1-acethyltransferase activities and decreasing ornithine decarboxylase mRNA level,[19] and they concluded that deferasirox has powerful antineoplastic effects and blocks cell proliferation in neoplastic cells by a pathway different from that of other iron chelators. However, they only refer to a limited number of reports regarding antiproliferative effect on human leukemia cells. Iron is critical for DNA synthesis and energy

doi: 10.1111/j.1349-7006.2009.01131.x

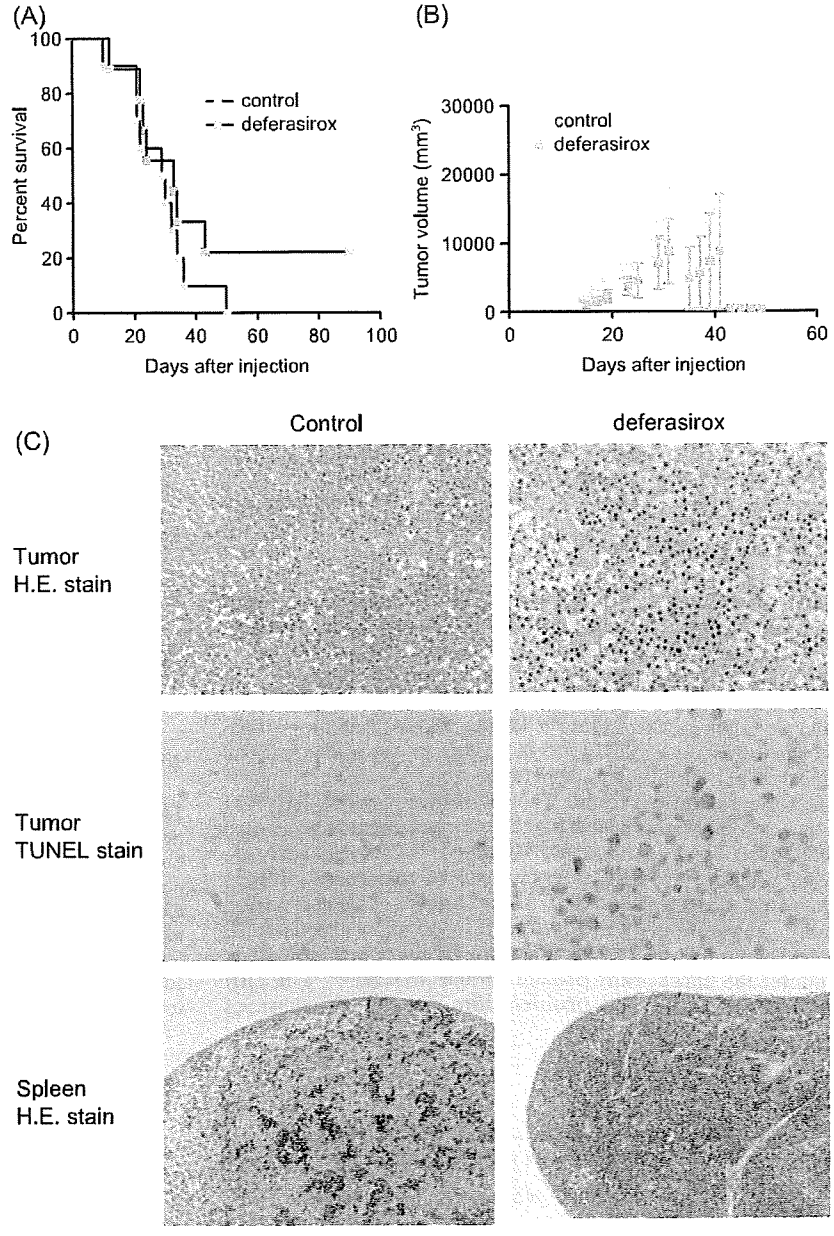

Fig. 5. *In vivo* effect of deferasirox in U937 xenografts. (A) Nude mice inoculated with 5×10^6 of U937 cells subcutaneously. Oral administration of deferasirox (50 mg/kg) or distilled water (control) was started 24 h after U937 injection. Oral administration of deferasirox induced some, but not significant, prolongation, of tumor-bearing mice ($P = 0.2450$). (B) Orally administered deferasirox inhibited the growth of U937 cells *in vivo*. Tumor volume (TV) was calculated for each individual mouse from the recorded caliper measurements of the longest (L) and shortest (L) dimensions (expressed in mm) of the one approximately ellipsoid tumor, according to the following formula: TV (mg) = $(W^2 \times L)/2$. A significant reduction of tumor volume was noted in desferasirox-treated mice ($P < 0.0001$). (c) Representative photographs of biopsy samples from mice treated for 23 days with phosphate buffered saline (PBS) (control) or deferasirox. H&E: hematoxyline-eosine; TUNEL, TdT-mediated dUTP nicked-end labeling. Original magnification ×200.

production, and neoplastic cells require more iron for their rapid proliferation.[2] Iron depletion inhibits iron-containing enzymes, ribonucleotide reductase, and up-regulates proapoptic proteins, Bax, caspase-3, caspase-8, and caspase-9 that induce apoptosis. Recently, orally available deferasirox has been given to patients with MDS to prevent excess iron deposition. Evidence suggests that iron chelation therapy actually reduces transfusion requirements, and improves some hematological findings in a subset of MDS patients, regardless of the percentage of blasts.[21] These findings lead us to consider molecular mechanisms of iron chelation by which proliferation of leukemic cells are inhibited.

In the current study, we demonstrated the cytotoxic effects due to apoptosis in human leukemia cell lines and freshly obtained leukemia cells from AML patients. The IC_{50} value of these cells ranged from 17 μM to 50 μM in leukemia cell lines and 87 μM to 172 μM in fresh leukemia cells. Since the phase I study of deferasirox treatment for heavily transfused patients receiving daily oral deferasirox of 20 mg/kg (the recommended dose for iron chelation therapy) demonstrated that 100 μM could be achieved *in vivo*,[22] the pharmacological dose of the antiproliferative effect *in vitro* is considered to be reasonable.

Gene expression profiling in deferasirox-treated K562 cells clarified up-regulation of several pathways which may reflect molecular mechanisms of iron chelator in human myeloid leukemia cells. The most prominent molecular feature is the up-regulation of *CDKN1A* encoding $p21^{CIP}$, which is consistent with the observation by Fu *et al.*[23] Deferroxamine paradoxically up-regulated $P21^{CIP1/WAF1}$ mRNA and down-regulates protein expression due to inhibition of the translocation of the $P21^{CIP1/WAF1}$ pathway and the induction of ubiquitin-independent proteasome degradation. We also noticed another pathway related to interferon. Several investigators have reported a possible association of iron chelation and inferferon.[24–26] Regis *et al.* reporter that iron regulates T-lymphocyte sensitivity to the IFN-gamma/Signal transducer

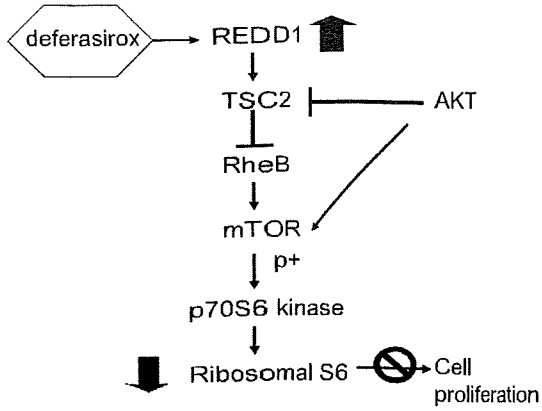

Fig. 6. Schematic model of REDD1/mTOR (mammalian target of rapamycin) pathways in deferasirox-treated K562 cells. The thicker arrow indicates the effect of deferasirox. When deferasirox is given, dephosphorylation of mTOR followed by up-regulation of the REDD1/tuberous sclerosis complex 2 (TSC2) pathway, induces down-regulation of ribosomal S6 protein, thereby, inhibiting cell proliferation.

and activator of transcription (STAT1) signaling pathway *in vitro* and *in vivo*.[24] More recently, Mori *et al.* found that expression of IFN-gammaR2 is restored by iron chelation, deferoxamine, and the increased expression of IFN-gammaR2 enhances the antiproliferative effect of IFN-gamma through induction of apoptosis in colon cancer cells.[26] Taking those findings together, the IFN pathway may partly be involved in the process of the anticancer effect during iron chelation.

In the current study, we found a novel pathway involving REDD1 which has recently been identified as a stress-response gene and is strongly induced by hypoxia,[27] (Fig. 6). REDD1 can activate the TSC2 protein:[28,29] TSC is composed of two proteins, TSC1 (also known as hamartin) and TSC2 (also known as tuberin), which function to integrate growth factors and cell stress responses. It has been shown that the major function of the TSC1/2 complex is to inhibit the checkpoint protein kinase mTOR,[28,30] a major regulator of cell death and proliferation. The mTOR enhances translational initiation in part by phosphorylating two major targets, the eIF4E binding protein (4E-BPs) and the ribosomal protein S6 (S6K1 and S6K2) that cooperate to regulate translational initiation rates.[30–33]

To the best of our knowledge, we have for the first time shown up-regulation of REDD1 expression in human leukemia cells treated with deferasirox. The REDD1 gene is strongly induced under hypoxic conditions in a hypoxia-inducible factor-1 (HIF-1)-dependent manner.[34] We demonstrated down-regulation of mTOR following up-regulation of REDD1, and marked down-regulation of the phosphorylated S6 protein in deferasirox-treated leukemia cells. Blockage of the REDD1 expression by siRNA resulted in restoration of mTOR and phosporylation of S6 protein in deferasirox-treated leukemia cells, indicating that the pathway involving mTOR might be important for cytotoxicity in the presence of iron chelating agents. These data provide valuable insights for novel therapeutic approaches aimed at the REDD1/mTOR pathway in human myeloid leukemia cells by means of iron chelation.

Although deferasirox may affect multiple pathways related to cell survival, more importantly, we demonstrated that deferasirox can induce apoptosis in xenotransplatable human leukemia cells in tumor-bearing mice. Our results may provide new insights into the complex molecular mechanism of iron chelation in human myeloid leukemia cells. Deferasirox might have benefit for not only iron chelation but also be an antiproliferative agent in some myeloid leukemia cells, especially in patients with myelodysplastic syndrome who need both iron chelation and reduction of leukemia cells.

Acknowledgments

The authors are indebted to Professor J. Patrick Barron of the International Medical Communications Center of Tokyo Medical University for his review of this manuscript. The authors also wish to thank Mr Yoshinobu Kamimura for his technical assistance. This work was supported by the 'Strategic Research Based Support' Project for private universities: matching fund subsidy from the MEXT (Ministry of Education, Culture, Sports, Science and Technology, 2008–12), and by the 'University-Industry Joint Research Project' for private universities: matching fund subsidy from the MEXT, 2007–09 (to KO, JHO).

References

1 Zhang AS, Enns CA. Iron homeostasis: recently identified proteins provide insight into novel control mechanisms. *J Biol Chem* 2008; August 29 [Epub ahead of print].
2 Andrews NC. Forging a field: the golden age of iron biology. *Blood* 2008; **112**: 219–30.
3 Domenico I, McVey Ward D *et al.* Regulation of iron acquisition and storage: consequences for iron-linked disorders. *Nat Rev Mol Cell Biol* 2008; **9**: 72–81.
4 Brard L, Granai CO, Swamy N. Iron chelators deferoxamine and diethylenetriamine pentaacetic acid induce apoptosis in ovarian carcinoma. *Gynecol Oncol* 2006; **100**: 116–27.
5 Yu Y, Wong J, Lovejoy DB *et al.* Chelators at the cancer coalface: desferrioxamine to Triapine and beyond. *Clin Cancer Res* 2006; **12**: 6876–83.
6 Kalinowski DS, Sharpe PC, Bernhardt PV *et al.* Design, synthesis, and characterization of novel iron chelators: structure-activity relationships of the 2-benzoypyridine thiosemicarbazone series and their 3-nitrobenzoyl analogues as potent antitumor agents. *J Med Chem* 2007; **50**: 3716–29.
7 Triantafyllou A, Liakos P, Tsakalof A *et al.* The flavonoid quercetin induces hypoxia-inducible factor-1alpha (HIF-1alpha) and inhibits cell proliferation by depleting intracellular iron. *Free Radic Res* 2007; **41**: 342–56.
8 Gharagozloo M, Khoshdel Z, Amirghofran Z. The effect of an iron (III) chelator, silybin, on the proliferation and cell cycle of Jurkat cells: a comparison with desferrioxamine. *Eur J Pharmacol* 2008; **589**: 1–7.
9 Cilloni D, Rosso V, Messa E *et al.* The oral ironchelator ICL670 is a otent inhibitor of NF-KB and this activity is independent from iron overload in MDS cells. *Haematologica* 2007; **s1**: 238.
10 Messa E, Defilippi I, Roetto A *et al.* Deferasirox is the only iron chelator acting as a potent NF-KB inhibitor in myelodysplastic syndromes. *Blood* (50th ASH Annual Meeting and and Exposition: 2008, Dec 6 to 9, San Francisco), abstract # 2671.
11 Choudhari SR, Khan MA, Harris G *et al.* Deactivation of Akt and STAT3 signaling promotes apoptosis, inhibits proliferation, and enhances the sensitivity of hepatocellular carcinoma cells to an anticancer agent, Atiprimod. *Mol Cancer Ther* 2007; **6**: 112–21.
12 Zhang Y, Ohyashiki JH, Takaku T *et al.* Transcriptional profiling of Epstein-Barr virus (EBV) genes and host cellular genes in nasal NK/T-cell lymphoma and chronic active EBV infection. *Br J Cancer* 2006; **94**: 599–608.
13 Ohyashiki JH, Hisatomi H, Nagao K *et al.* Quantitative relationship between functionally active telomerase and major telomerase components (hTERT and hTR) in acute leukaemia cells. *Br J Cancer* 2005; **92**: 1942–7.
14 Ohyashiki JH, Hamamura R, Kobayashi C, Zhang Y, Ohyashiki K. A network approach for anti-cancer effect of bortezmib identifies SPARC as a therapeutic target in adult T-cell leukemia cells. *Computational Biol Chem Adv Appl* 2008; **1**: 85–93.
15 Akahane D, Tauchi T, Okabe S *et al.* Activity of a novel Aurora kinase inhibitor against the T315I mutant form of BCR-ABL. in vitro and in vivo studies. *Cancer Sci* 2008; **99**: 1251–7.
16 Richardson DR, Tran EH, Ponka P. The potential of iron chelators of the pyridoxal isonicotinoyl hydrazone class as effective antiproliferative agents. *Blood* 1995; **86**: 4295–306.
17 Valle P, Timeus F, Piglione M *et al.* Effect of different exposures to desferrioxamine on neuroblastoma cell lines. *Pediatr Hematol Oncol* 1995; **12**: 439–46.
18 Darnell G, Richardson DR. The potential of iron chelators of the pyridoxal isonicotinoyl hydrazone class as effective antiproliferative agents III. the effect of the ligands on molecular targets involved in proliferation. *Blood* 1999; **94**: 781–92.
19 Chaston TB, Lovejoy DB, Watts RN *et al.* Examination of the

doi: 10.1111/j.1349-7006.2009.01131.x

antiproliferative activity of iron chelators: multiple cellular targets and the different mechanism of action of triapine compared with desferrioxamine and the potent pyridoxal isonicotinoyl hydrazone analogue 311. *Clin Cancer Res* 2003; **9**: 402–14.
20 Lescoat G, Chantrel-Groussard K, Pasdeloup N *et al.* Antiproliferative and apoptotic effects in rat and human hepatoma cell cultures of the orally active iron chelator ICL670 compared to CP20: a possible relationship with polyamine metabolism. *Cell Prolif* 2007; **40**: 755–67.
21 Chantrel-Groussard K, Gaboriau F *et al.* The new orally active iron chelator ICL670A exhibits a higher antiproliferative effect in human hepatocyte cultures than O-trensox. *Eur J Pharmacol* 2006; **541**: 129–37.
22 Miyazawa K, Ohyashiki K, Urabe A *et al.* A safety, pharmacokinetic and pharmacodynamic investigation of deferasirox (Exjade, ICL670) in patients with transfusion-dependent anemias and iron-overload: a Phase I study in Japan. *Int J Hematol* 2008; **88**: 73–81.
23 Fu D, Richardson DR. Iron chelation and regulation of the cell cycle: 2 mechanisms of posttranscriptional regulation of the universal cyclin-dependent kinase inhibitor $p21^{CIP1/WAF1}$ by iron depletion. *Blood* 2007; 110: 752–61.
24 Regis G, Bosticardo M, Conti L *et al.* Iron regulates T-lymphocyte sensitivity to the IFN-gamma/STAT1 signaling pathway in vitro and in vivo. *Blood* 2005; **105**: 3214–21.
25 Okada T, Sawada T, Kubota K. Deferoxamine enhances anti-proliferative effect of interferon-gamma against hepatocellular carcinoma cells. *Cancer Lett* 2007; **248**: 24–31.
26 Mori S, Sawada T, Okada T, Kubota K. Anti-proliferative effect of interferon-gamma is enhanced by iron chelation in colon cancer cell lines in vitro. *Hepatogastroenterology* 2008; **55**: 1274–9.
27 Schwarzer R, Tondera D, Arnold W *et al.* REDD1 integrates hypoxia-mediated survival signaling downstream of phosphatidylinositol 3-kinase. *Oncogene* 2005; **24**: 1138–49.
28 Nobukini T, Thomas G. The mTOR/S6K signalling pathway. the role of the TSC1/2 tumour suppressor complex and the proto-oncogene Rheb. *Novartis Found Symp* 2004; **262**: 148–54; discussion 154–9, 265–8.
29 Wang H, Kubica N, Ellisen LW *et al.* Dexamethasone represses signaling through the mammalian target of rapamycin in muscle cells by enhancing expression of REDD1. *J Biol Chem* 2006; **281**: 39128–34.
30 Li Y, Corradetti MN, Inoki K *et al.* filling the GAP in the mTOR signaling pathway. *Trends Biochem Sci* 2004; **29**: 32–8.
31 Corradetti MN, Inoki K, Guan KL. The stress-inducted proteins RTP801 and RTP801L are negative regulators of the mammalian target of rapamycin pathway. *J Biol Chem* 2005; **280**: 9769–72.
32 Jin HO, An S, Lee HC *et al.* Hypoxic condition- and high cell density-induced expression of Redd1 is regulated by activation of hypoxia-inducible factor-1alpha and Sp1 through the phosphatidylinositol 3-kinase/Akt signaling pathway. *Cell Signal* 2007; **19**: 1393–403.
33 Wang H, Kubica N, Ellisen L *et al.* Dexamethasone represses signaling through the mammalian target of Rapamycin in muscle cells by enhancing expression of REDD1. *J Biol Chem* 2006; **51**: 39128–34.
34 Wouters BG, Koritzinsky M. Hypoxia signalling through mTOR and the unfolded protein response in cancer. *Nat Rev Cancer* 2008; **8**: 851–64.
35 Shoshani T, Faerman A, Mett I *et al.* Identification of a novel hypoxia-inducible factor 1-responsive gene, RTP801, involved in apoptosis. *Mol Cell Biol* 2002; **22**: 2283–93.

Supporting Information

Additional Supporting Information may be found in the online version of this article:

File S1. Western blot analysis of U937 and HL60 with or without treatment by deferasirox: Expression of phosphorylated S6 ribosomal protein was decreased in the presence of deferasirox.

Please note: Wiley-Blackwell are not responsible for the content or functionality of any supporting materials supplied by the authors. Any queries (other than missing material) should be directed to the corresponding author for the article.

Leukemia Research 33 (2009) 756–758

Contents lists available at ScienceDirect

Leukemia Research

journal homepage: www.elsevier.com/locate/leukres

Evaluation of cardiac iron overload in transfusion-dependent adult marrow failure patients by magnetic resonance imaging

Jinho Park[a], Kazuma Ohyashiki[b,*], Soichi Akata[a], Kenichi Takara[a], Ritsuko Uno[a], Dai Kakizaki[a], Keisuke Miyazawa[b], Yukihiko Kimura[b], Koichi Tokuuye[a]

[a] Department of Radiology, Tokyo Medical University, Tokyo 160-0023, Japan
[b] First Department of Internal Medicine (Division of Hematology), Tokyo Medical University, 6-7-1 Nishishinjuku, Shinjuku-ku, Tokyo 160-0023, Japan

ARTICLE INFO

Article history:
Received 2 September 2008
Received in revised form 14 October 2008
Accepted 20 October 2008
Available online 26 November 2008

Keywords:
Iron overload
Myocardial evaluation
MRI
Transfusion-dependent

ABSTRACT

We investigated magnetic resonance imaging T2-star (MRI-T2*) values and left ventricular ejection fraction (LVEF) in 7 adult patients with bone marrow failure with heavy transfusion to elucidate the correlation between cardiac iron overload and dysfunction. We demonstrated a positive correlation between the total volume of red blood cells (RBC) transfusion and ejection fraction. The normal T2* limit value, which represents cardiac siderosis, is probably 200 mL/kg RBC transfusion. Patients with serum ferritin levels of under 5000 ng/mL and who received 200–400 mL/kg RBC transfusion showed mild but progressive decrease of the T2* value without obvious reduction of the ejection fraction, indicating that the T2* value of MRI could be a predictor for cardiac iron deposition before the appearance of myocardial dysfunction. Transfused RBC amount of >400 mL/kg or rapid elevation of ferritin level of >5000 ng/mL might be warning sign for critical cardiac dysfunction. Since iron overload of the heart is a major factor affecting co-morbidity of bone marrow failure, MRI evaluation of cardiac iron overload and functional disturbance in adult non-thalassemic patients is essential.

1. Introduction

Iron overload is a major problem in managing patients with bone marrow failure syndromes, since it has been clarified that cardiac dysfunction is a major life-threatening co-morbidity [1]. Takatoku et al. demonstrated that most of the deaths of iron overload adult patients with marrow failure syndromes were due to infection and leukemia; while cardiac and liver failure were noted in 24.0% and 6.7%, respectively [1]. Therefore, early detection of cardiac iron overload before apparent cardiac dysfunction, and chelation therapy for patients receiving heavy transfusion with acquired anemia is recommended. In the past, a limited number of studies regarding myocardial iron overload in adult patients with transfusion-dependent acquired anemias have been published [2–7]. Some reports suggested that the cardiac magnetic resonance imaging T2-star (MRI-T2*) technique could be useful in determining cardiac iron overload [3,7], while the efficacy of MRI is still controversial [2]. We, therefore, planned to address this relevant clinical issue.

2. Materials and methods

2.1. Patients

We studied 7 adult patients with hematologic diseases, all of whom were transfusion-dependent. Total red cell transfusion value at the time of MRI evaluation ranged from 64 (12,800 mL) to 242 (48,400 mL) Japanese units (1 unit = 200 mL) of red blood cells (RBC). Serum ferritin levels ranged from 2868 ng/mL to 17,547 ng/mL at the time of the MRI study. Of the 7 patients, 2 each was given a diagnosis of diabetes mellitus or liver dysfunction (Table 1). None of the patients in this study received oral chelation therapy, but all of them received intermittent intravenous deferoxamine therapy.

2.2. MRI evaluation

We used a Magnetom Avanto 1.5 T scanner (Siemens AG, Erlangen, Germany) using a gradient echo T2* MRI technique. Gradient echo (GRE) T2*WI, and true-fast imaging with steady-state procession (true FISP) sequence was applied for a single mid-ventricular short-axis slice of the left cardiac ventricle at seven echo times (5 ms, 7 ms, 10 ms, 13 ms, 15 ms, 17 ms and 20 ms). The repeat time between each radiofrequency pulse was 170 ms. Phased array coils, electrocardiogram (ECG) gating, and breath holding methods were also utilized. We selected the short-axis of the left cardiac ventricle and applied true-FISP sequence to obtain cine MRI.

All MRI data were analyzed using Argus soft ware (Siemens AG) to calculate left ventricular ejection fraction (LVEF). Regions of interest (ROI) were set to the left ventricle wall. Measured signal intensity was fitted for an exponential curve and we obtained the T2* value of the myocardium. Axial T2*WI of upper abdomen was also obtained to determine the amounts of iron deposition in other organs, including the liver, pancreas, spleen, and vertebrae.

* Corresponding author. Tel.: +81 3 3342 1510; fax: +81 3 5381 6651.
E-mail address: ohyashik@rr.iij4u.or.jp (K. Ohyashiki).

0145-2126/$ – see front matter © 2008 Elsevier Ltd. All rights reserved.
doi:10.1016/j.leukres.2008.10.018

Table 1
Clinico-hematologic characteristics of patients with iron overload.

UPN	Age (yo)/sex	Diagnosis	Hb (g/dL)	Platelets ($\times 10^3$/L)	Total RBC transfusion (Japanese unit)	Serum ferritin (ng/mL)	Fe (μg/dL)	T2* value (ms)	LVEF (%)
1	56/male	MDS-RAEBt	7.7	31	12,800 mL (64)	3,056	171	94.34	61
2	71/female	MDS-RA	5.1	158	32,000 mL (160)	16,987	334	ND	52.8
3	66/male	MDS-RA	7.9	15	23,200 mL (116)	3,856	ND	35.71	63
4	37/female	AA	7.9	3	48,400 mL (242)	17,547	379	11.55	26.5
5	52/female	AA	8.2	11	>12,800 mL (>64)	3,441	233	50	54.8
6	77/male	PMF	7.2	34	11,600 mL (58)	2,868	152	51.02	59.5
7	71/male	PMF	4.6	212	24,000 mL (120)	3,176	300	35.59	61.3

Disease: MDS-RA, myelodysplastic syndrome-refractory anemia; MDS-RAEBt, myelodysplastic syndrome-refractory anemia with excess blasts in transformation; AA, aplastic anemia; PMF, primary myelofibrosis. Patient 5 had a diagnosis at childhood, thus exact transfused amount is unclear.

3. Results

Left ventricular ejection fraction in the 7 patients ranged from 26.5% to 63% (normal range: 56–78% by MRI), with 3 (patient nos. 2, 4, and 5) of them being below the normal range. Two (patient nos. 2 and 4) of the 3 patients with reduced LVEF levels had heavy RBC transfusion of >160 Japanese units and the serum ferritin levels were >15,000 ng/mL. Although the remaining 4 transfusion-dependent patients showed ferritin levels of around 3000 ng/mL, none of them showed marked reduction of LVEF, except patient 5 who was given a diagnosis of aplastic anemia in childhood and in whom the exact transfused RBC amount could not be calculated.

Because of blurring artifacts, we measured cardiac T2* value in 6 patients. Breath holding was difficult for patient no. 2 and we therefore failed to establish the ROI in the myocardium of this patient. Although the number of patients in this study is too small to provide a definite conclusion, we were able to note some tendencies regarding iron overload in the heart. Two patients (nos. 1 and 6) who received relatively small amounts of RBC transfusions (approximately 60 Japanese units: 12,000 mL) had normal T2* value, suggesting that at 60 units RBC (200 mL/kg) transfusion myocardial iron overload may not occur. Most patients with RBC transfusion of 60–120 units (200–400 mL/kg) maintained normal LVEF, while some of them demonstrated mild reduction in T2* value (35.71 ms and 35.59 ms); but the above 2 patients (nos. 3 and 7) with 60 units of transfusion showed the limit of the normal range T2* value reported by Anderson et al., i.e., 52 ± 16 ms [7]. These data indicate that some patients with heavy transfusion of 60–120 RBC Japanese units (12,000–24,000 mL RBC) may not be detectable myocardial damage by LVEF alone, and the T2* value of MRI could show cardiac iron deposition before the appearance of myocardial dysfunction.

We utilized GraphPad Prism 5.0 software (GraphPad Software Inc., San Diego, CA, USA) to obtain non-lineal fitting capabilities between total transfused RBC volume and serum ferritin, T2* value, or ejection fraction by MRI (Fig. 1).

(1) *No obvious cardiac siderosis*: patients with RBC transfusion of <200 mL/kg (<12,000 mL RBC) exhibiting elevated serum ferritin up to 4000 ng/mL, normal T2* value (36–68 ms), and normal LVEF (56–78% by MRI).
(2) *Cardiac siderosis*: patients with RBC transfusion of 200–400 mL/kg (12,000–24,000 mL RBC) exhibiting elevated serum ferritin up to 4000 ng/mL, progressive reduction of the T2* value, and normal LVEF (56–78% by MRI).
(3) *Cardiac dysfunction due to siderosis*: patients with RBC transfusion of >400 mL/kg (>24,000 mL) exhibiting elevated serum ferritin levels of more than 15,000 ng/mL, reduced T2* value (<20 ms), and abnormal LVEF (<56% by MRI).

4. Discussion

In the current study, we failed to demonstrate a linear correlation between the T2* value and left ventricular ejection fraction, especially in patients with transfusion of less than 120 Japanese units of RBC (<400 mL/kg). Approximately 50% of them showed some reduction of T2* value, while most of them exhibited a normal LVEF, indicating that these high transfusion level patients are at high risk for developing cardiac dysfunction, and detection of insidiously progressive dysfunction detected by MRI might be important for those patients. The situation is similar in those with serum ferritin levels between 2000 ng/mL and 4000 ng/mL: evaluation of LVEF alone by echocardiogram may fail to find out the pre-existing myocardial damage due to iron overload.

The T2* value is related to not only iron deposition but also fibrosis, and MRI reflects total images of these pathologic changes. Currently iron chelation therapy for hematologic disease patients, especially those with myelodysplastic syndromes (MDS), with transfusion-dependency is recommended [3], and definitions of iron overload for MDS patients have been proposed [8,9]. Although the starting point for iron chelation therapy is proposed, the exact evaluation of iron overload and functional estimation in each organ is probably important. Reduction of iron deposition in mouse organs by chelation therapy was demonstrated [10]. Thus, improvement of cardiac siderosis and myocardial dysfunction by chelation therapy should be determined.

Anderson et al. reported cardiac iron deposition in 109 thalassemia patients with iron chelation therapy and found significant ventricular dysfunction in patients with myocardial T2* values of less than 20 ms, and progressive decline in ejection fraction [7].

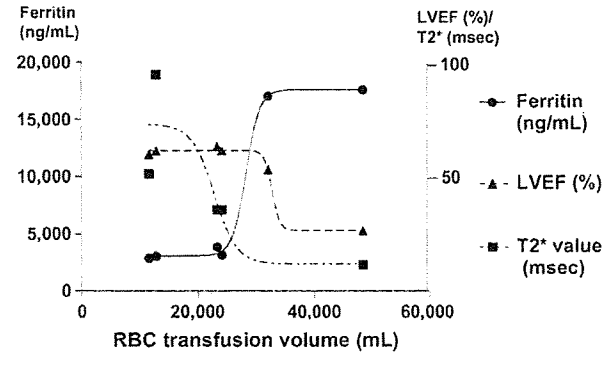

Fig. 1. Correlation between total units of red blood cell transfusion (horizontal axis) and left ventricular ejection fraction (LVEF), serum ferritin, and cardiac T2* value using GraphPad Prism 5.0 software. Rapid decline of T2* value, but stable LVEF within the normal range until 400 mL/kg of red blood cell transfusion and serum ferritin level of <5000 ng/mL are notable. The rapid decline of LVEF following rapid elevation of serum ferritin is evident.

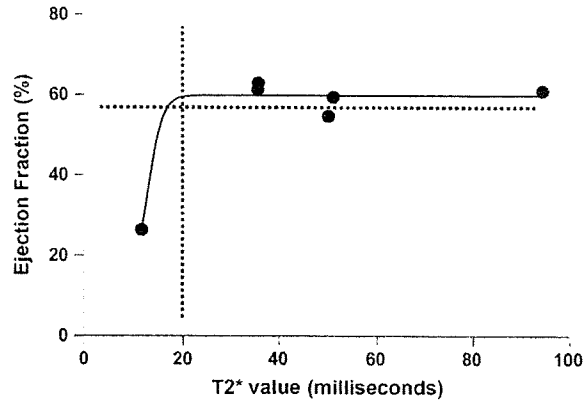

Fig. 2. Correlation between cardiac T2* value and left ventricular ejection fraction. The vertical dotted line indicates the cut-off value of T2* (20 ms) and the horizontal dotted line shows the cut-off value of LVEF (56%) for cardiac dysfunction.

In contrast, Jensen et al. failed to demonstrate significant correlation between cardiac T2* value and serum ferritin levels [5]. More recently, Di Tucci et al. reported myocardial iron overload detected by MRI in adult transfusion-dependent acquired anemias and found cardiac T2* value correlated with transfusion burden, and suggested that 290 mL/kg RBC might be a cut-off for myocardial damage [6]. Our results show that patients who received transfusions of up to 24,000 mL RBC (approximately 400 mL/kg) had a progressive decrease of the T2* value, but most of them had a normal left ventricular ejection fraction. These data clearly indicate that patients receiving 200–400 mL/kg RBC transfusion with moderate reduction of T2* value, but not less than 20 ms, in acquired anemia patients with heavy transfusion may be at high risk for progressive cardiac dysfunction (Fig. 2).

In conclusion, RBC transfusion of 200 mL/kg RBC might be the limit for monitoring normal T2* values. Patients who received 200–400 mL/kg RBC transfusion showed progressive decrease of T2* value without obvious reduction of ejection fraction, indicating that the T2* value of MRI could indicate cardiac iron deposition before apparent myocardial dysfunction. Patients who had received ≥400 mL/kg RBC transfusion eventually showed progressive cardiac failure.

Conflicts of interest

The authors declare no conflicts of interests.

Acknowledgements

Thanks are due to Prof. J. Patrick Barron, salaried employer of Tokyo Medical University, for his review of this manuscript. We also thank to Mr. H. Katsuyama and Y. Araki, Department of Radiology, Tokyo Medical University, Y. Komori, Siemens-Asahi Medical Technologies Ltd., Japan, for their technical help and Dr. J. H. Ohyashiki, Intractable Diseases Research Center, for statistical analysis. This work was supported in part by a Grant-in-Aid from Japanese Ministry of Health, Labor and Welfare.

References

[1] Takatoku M, Uchiyama T, Okamoto S, et al. Japanese National Research Group on Idiopathic Bone Marrow Failure Syndromes. Retrospective nationwide survey of Japanese patients with transfusion-dependent MDS and aplastic anemia highlights the negative impact of iron overload on morbidity/mortality. Eur J Haematol 2007;78:487–94.
[2] Konen E, Ghoti H, Goitein O, et al. No evidence for myocardial iron overload in multitransfused patients with myelodysplastic syndrome using cardiac magnetic resonance T2 technique. Am J Hematol 2007;82:1013–6.
[3] Greenberg PL. Myelodysplastic syndromes: iron overload consequences and current chelating therapies. J Natl Compr Cancer Netw 2006;4:91–6.
[4] Chacko J, Pennell DJ, Tanner MA, et al. Myocardial iron loading by magnetic resonance imaging T2* in good prognostic myelodysplastic syndrome patients on long-term blood transfusions. Br J Haematol 2007;138:587–93.
[5] Jensen PD, Jensen FT, Christensen T, et al. Evaluation of myocardial iron by magnetic resonance imaging during iron chelation therapy with deferrioxamine: indication of close relation between myocardial iron content and chelatable iron pool. Blood 2003;101:4632–9.
[6] Di Tucci AA, Matta G, Deplano S, et al. Myocardial iron overload assessment by T2* magnetic resonance imaging in adult transfusion dependent patients with acquired anemias. Haematologica 2008;93:1358–8.
[7] Anderson LJ, Holden S, Davis B, et al. Cardiovascular T2-star (T2*) magnetic resonance for the early diagnosis of myocardial iron overload. Eur Heart J 2001;22:2171–9.
[8] Gatterman N. Guidelines on iron chelation therapy in patients with myelodysplastic syndromes and transfusional iron overload. Leuk Res 2007;(Suppl. 3):S10–5.
[9] Suzuki T, Tomonaga M, Miyazaki Y, et al. Japanese epidemiological survey with consensus statement on Japanese guidelines for treatment of iron overload in bone marrow failure syndromes. Int J Hematol 2008;88:30–5.
[10] Wood JC, Otto-Duessel M, Gonzalez I, et al. Deferasirox and deferiprone remove cardiac iron in the iron-overload gerbil. Transl Res 2006;148:272–80.

Biochemical and Biophysical Research Communications 383 (2009) 245–251

Contents lists available at ScienceDirect

Biochemical and Biophysical Research Communications

journal homepage: www.elsevier.com/locate/ybbrc

Identification of a common microdeletion cluster in 7q21.3 subband among patients with myeloid leukemia and myelodysplastic syndrome

Hiroya Asou, Hirotaka Matsui, Yuko Ozaki, Akiko Nagamachi, Megumi Nakamura, Daisuke Aki, Toshiya Inaba *

Department of Molecular Oncology and Leukemia Program Project, Research Institute for Radiation Biology & Medicine, Hiroshima University, 1-2-3 Kasumi, Minami-ku, Hiroshima 734-8553, Japan

ARTICLE INFO

Article history:
Received 31 March 2009
Available online 7 April 2009

Keywords:
Monosomy 7
Myeloid malignancy
Tumor suppressor
Mitosis

ABSTRACT

Monosomy 7 and interstitial deletions in the long arm of chromosome 7 (−7/7q−) is a common nonrandom chromosomal abnormality found frequently in myeloid disorders including acute myeloid leukemia (AML), myelodysplastic syndrome (MDS), and juvenile myelomonocytic leukemia (JMML). Using a short probe-based microarray comparative genomic hybridization (mCGH) technology, we identified a common microdeletion cluster in 7q21.3 subband, which is adjacent to 'hot deletion region' thus far identified by conventional methods. This common microdeletion cluster contains three poorly characterized genes; *Samd9*, *Samd9L*, and a putative gene *LOC253012*, which we named *Miki*. Gene copy number assessment of three genes by real-time PCR revealed heterozygous deletion of these three genes in adult patients with AML and MDS at high frequency, in addition to JMML patients. Miki locates to mitotic spindles and centrosomes and downregulation of Miki by RNA interference induced abnormalities in mitosis and nuclear morphology, similar to myelodysplasia. In addition, a recent report indicated Samd9 as a tumor suppressor. These findings indicate the usefulness of the short probe-based CGH to detect microdeletions. The three genes located to 7q21.3 would be candidates for myeloid tumor-suppressor genes on 7q.

Introduction

Monosomy 7 and interstitial deletions in 7q (−7/7q−) are a common nonrandom chromosomal abnormality found frequently in myeloid disorders. In 1964, prior to chromosome band identification, monosomy 7 was first reported in three patients with refractory anemia as monosomy of a C-group chromosome [1]. Since that time, −7/7q− have been identified in 10–20% of a wide range of myeloid malignancies including MDS, AML, and JMML [2].

Enormous efforts have been made to identify genes responsible for −7/7q−. In the absence of definitive familial cases, the basic strategy for gene hunting began with identifying patients that carried 7q−. Detailed maps of regions deleted from individual patients were then generated from the results of loss of heterogeneity assays or fluorescence *in situ* hybridization. Unfortunately, the cumulative results from thousands of patients were confounded by the fact that the boundaries of commonly deleted regions derived by separate research groups showed a poor degree of overlap [3]. Currently, it is generally accepted that two or more genes near bands 7q22 and/or 7q34 are involved in myeloid tumors.

Microarray-based comparative genomic hybridization (mCGH) technology allows efficient detection of microdeletions (<100 kb) that affect one or a few genes, enabling to search for small 7q deletions that are not visible cytogenetically in marrow cells of MDS/AML patients. Initially, bacterial artificial chromosome (BAC)-based mCGH systems were developed, but this system had limited potential to detect microdeletions because of the long probe size (>100 kb). Thereafter, SNP-array hybridization turned out to be a powerful method for detecting not only single nucleotide polymorphism, but also microdeletions [4]. However, because SNPs tend to cluster within introns and intergenic spaces, SNP-array may bias against the detection of microdeletions in critical genes.

Here, we describe the application of a modified BAC-based mCGH system that uses short (<10 kb) genomic DNA fragments without any repetitive sequences as probes to improve the detection of small deletions and reduce background hybridization. Because repeat-free fragments generally overlap exon-containing regions, this type of probe not only yields a high signal/noise ratio, but also can be useful in determining the copy number of a corresponding gene. Using this system for identification of responsible gene(s) for −7/7q−, we report the isolation of a common microde-

* Corresponding author. Fax: +81 82 256 7103.
E-mail address: tinaba@hiroshima-u.ac.jp (T. Inaba).

0006-291X/$ - see front matter © 2009 Elsevier Inc. All rights reserved.
doi:10.1016/j.bbrc.2009.04.004

letion among JMML patients that contains three poorly characterized genes.

Materials and methods

Short probe-based mCGH. This system was similar to that described by others [5]. Briefly, total 292 repeat-free segments (2.7–9.5 kb) were identified using BlastN at the NCBI server (235 probes in 7q21.2–7q31.1, 15 in 4q12, 27 in 20q, and 15 in 21q). Each of these fragments was PCR amplified from human placenta DNA (Clontech, Mountain View, CA) and cloned into the pCR-XL-TOPO vector (Invitrogen, Carlsbad, CA). The primer sets used to amplify probes #14–#16 are listed in Table 1. Sequences of other primer sets are available upon request. Five micrograms of each target DNA, PCR-amplified fragments using universal primers in the vector, was printed on poly-L-lysine coated glass slides (Matsunami Glass, Osaka, Japan) using a spotter (SPBIO, Hitachi Software, Tokyo, Japan). Bone marrow samples were obtained after informed consent and approval from the Institutional Review Board at Hiroshima University. Test samples and reference placenta DNA (2.5 μg) were random-prime labeled with CY3- and CY5-dCTP (GE healthcare), respectively, and then hybridized to the slide. Scanning of microarrays was performed using G2505A scanner (Agilent Technologies, Santa Clara, CA) and signals were analyzed with ArrayVision (GE healthcare).

Cell culture and gene transfer. EOL-1 and MUTZ-3 cells ([6] and references in it) were cultured in RPMI1640 medium with 10% (FBS). 293 and HeLa(tc) [7] cells were cultured in Dulbecco's modified Eagle's medium supplemented with 10% fetal bovine serum (FBS). siRNA oligonucleotides (100 nM, otherwise indicated, Table 2) were transfected using Oligofectamine (Invitrogen). C-terminal FLAG-tagged Mikiα or β protein, or MikiΔN-FLAG(C) protein (lacking N-terminal hydrophobic 30 aa of Mikiβ) was expressed using the pcDNA3 expression vector (Invitrogen).

Other experimental procedures and reagents. Copy number assessment by qPCR was performed according to the procedure described [8]. qRT-PCR was performed as previously described [9] using primer sets (Table 1). Immunoprecipitation and immunoblot analyses were performed according to the standard procedures [10] using 2% gelatin as a blocking agent. Immunostaining and image analyses were performed as described [7,11]. Rabbit anti-Miki antibodies was raised against GST-Mikiα (377–462 aa) and affinity purified according to the standard procedures [10].

Table 2
Target sequences for RNAi.

Name	Sequence
siRNA#79	CGGUUGAUGAUCCUGUCAC
siRNA#80	GGAAGACAUUGGGAAUUAC
siRNA#81	AGGCAUUUAUGCAAAUUGAA
shMiki#1	AUGCAUCUCUGCUUAUCAACC
shMiki#2	GAAGGCAAUUACAUCGUGAAG
shMiki#3	UCAGGGAAAUGGAACUCUAUC
shMiki#4	AGAAGACAAUGGACUAUGUGU
shMiki#5	GAAACUCAUUUCACAGUUAUC
shMiki#6	UGACUUCGGAAUAUAUGAAUU

Results

Identification of three candidate myeloid tumor-suppressor genes in a common microdeletion cluster among JMML patients

Two hundred thirty-five probes in a region spanning 21.7 Mb within 7q21.2–7q31.1 and additional 57 control probes in 4q, 20q, and 21q were applied to a search for microdeletions using a short probe-based mCGH system (see Materials and methods). Test (leukemia) and reference DNA samples were labeled with CY3- and CY5-dCTP, respectively, and then hybridized to slides on which probes were printed.

We initially tested whether this system can detect copy number changes in a small region. Genomic DNA extracted from EOL-1 cells, which is known to harbor a deletion spanning 800 Kb between the *Rhe* (*FIP1L1*) gene and the *PDGFα* gene in 4q [12]. All eight probes (#239–#246) that locate within the deletion showed low fluorescence ratios (Fig. 1A, bracket), demonstrating the potential of this system to detect microdeletions. For detection of microdeletion in myeloid leukemia cells, we selected fresh bone marrow samples from adult AML/MDS patients or DNA from myeloid leukemia cell lines that did not show apparent 7q abnormalities. However, as shown, for an example, in Fig. 1B, gross regional copy number changes were still detected, and 'single copy events', which could include both real copy number changes in a small region and noise of the system, were frequently observed, recognized as general problems in detection of microdeletions in leukemia cells [13]. We then applied the microarray CGH system to samples from JMML patients, which is a subtype of MDS and is occasionally associated with monosomy 7 [2]. In contrast to adult MDS/AML pa-

Table 1
Primer sets.

	Forward	Reverse
Probe#14	5′-AACTTCTCCTGACTCCAGTCATAGCTCCTT-3′	5′-ATCCATAGACCTGACATGTGTATCATATCC-3′
Probe#15	5′-GTGGGAATCGTCTACTTCCTGCACTCAAGA-3′	5′-TGATTAAAGACTGGACCAAAGAGCATGTGA-3′
Probe#16	5′-TGCTCACTCAACCGAAATCAATATTGAGAT-3′	5′-ATGCTTTAGGCTCCTAAGCCTTCTTTCCTT-3′
Top2b	5′-CAACTTTTTGCTGGCATCTG-3′	5′-GCTGGAATGTCTGGAAAAGC-3′
Tel	5′-ACAAATCACCGGCCTTCTCCTGACCC-3′	5′-GGCTGGATGGCTTCGGGTGGGACTC-3′
Albumin	5′-AGCTATCCGTGGTCCTGAAC-3′	5′-TTCTCAGAAAGTGTGCATATATCTG-3′
c7orf16	5′-CAGGCCCAGCCTCGGTGAGC-3′	5′-GCACAACCCCGTGCCACCAG-3′
DDC	5′-CTCATGGCTCACGCGTCCAG-3′	5′-CAAGCCGACCTAGGTTGGTG-3′
Cdk6	5′-ACACTGCCTTGTTGGCAAAG-3′	5′-AGGTTTGCAGAATCGAGGCC-3′
Samd9–5′	5′-AACCCAGATATGGCTAATCC-3′	5′-CAGGTCTATGGATGGTTGCC-3′
Samd9–3′	5′-CGTTTACAAGGTCGAGCTGA-3′	5′-CCCAGGTAAAAAGACACCTT-3′
Samd9L	5′-CATTCCTGTGCTTCTCCTTG-3′	5′-GGATTCCGGGATCTCATGCA-3′
Miki-5′	5′-CCTGGTGAGGAACCCTGTCA-3′	5′-TCTCTGTGACTATCCTGGGA-3′
Miki-3′	5′-CAAGGCATTCGGTTTGTAAG-3′	5′-CTCTGGTGAAGCAGAATTCT-3′
CCDC132	5′-AGGATACCCTGGGTCGGCTC-3′	5′-TTCAGCCGCCGCGACTTACC-3′
Col1A2	5′-GCAGTAACCTTATGCCTAGC-3′	5′-GAGAGTCTGCCCTCCAAGTG-3′
Rint-1	5′-GCTGAGTATGTCTGTTGAAG-3′	5′-CCAAACTAGATACAGGTGCC-3′
Lep	5′-GTATCTCCAGGATTGAAGAG-3′	5′-CCCACTCTTTGCTGGGTGGA-3′
Miki(RT)	5′-AACTCTATCTGCCAGTCAGAAG-3′	5′-TTTAGCCATTGGTAAGCTAGCC-3′
HPRT(RT)	5′-CCTCATGGACTAATTATGGACAG-3′	5′-GCAGGTCAGCAAAGAATTTATAG-3′